

Detection and attribution of short term ocean carbon cycle events using continuous measurements of CO₂, O₂ and APO from Mace Head Atmospheric Research Station, Ireland

by Alison Craggs
Student Number: 100105008

Thesis presented in part-fulfilment of the degree of Master of Science in accordance with the regulations of the University of East Anglia

School of Environmental Sciences
University of East Anglia
University Plain
Norwich
NR4 7TJ

© 2015 Alison Craggs

This copy of the dissertation has been supplied on condition that anyone who consults it is understood to recognise that its copyright rests with the author and that no quotation from the dissertation, nor any information derived there from, may be published without the author's prior written consent. Moreover, it is supplied on the understanding that it represents an internal University document and that neither the University nor the author are responsible for the factual or interpretative correctness of the dissertation.

Acknowledgements

I would like to thank my supervisor, Dr. Andrew Manning, for his invaluable guidance, support and advice throughout my project. I am very grateful to Penelope Pickers who has been incredibly patient and helpful in teaching me R programming, curve fitting programs and answering my questions. She kindly ran HPspline and CCGCRV and NAME for me.

For providing the Mace Head O₂ and CO₂ data, I thank Phil Wilson, Sander van der Laan, Penelope Pickers (all UEA) and Gerry Spain (University of Galway, Ireland); for providing Mace Head meteorology data, I thank Michel Ramonet (Laboratoire des Sciences du Climat et de l'Environnement, France).

Abstract

Anthropogenic emissions greenhouse gases are causing increasing global temperature and climate change. The ocean is the largest carbon sink and absorbs 40 % of anthropogenic CO₂ emissions. However, our understanding of the processes involved is still limited. This project aims to improve understanding of the ocean carbon cycle through the analysis of short term excursions above the baseline data (atmospheric events). This is achieved through the use of continuous atmospheric measurements of CO₂ and O₂ collected from Mace Head Atmospheric Research Station, Ireland. The season cycle amplitudes of the CO₂, O₂ and APO data are 17.78 ppm, 149 per meg and 76.57 per meg respectively. Six marine productivity related events and five upwelling or ventilation events were identified within the 13 month dataset. Seasonality is found in the magnitude of the events. The sign and strength of correlation of the oxidative ratios is found to indicate the dominant processes responsible for the atmospheric event. I used the air-sea fluxes calculated for these events to test conceptual models and found a good fit between the two flux estimates. Four of the modelled fluxes of productivity events are within the same order of magnitude of the APO derived fluxes, and the remaining two are an order of magnitude greater. In the majority of cases, including the heat fluxes increases the difference between APO-derived and modelled fluxes. For ventilation events the modelled and APO-derived fluxes are with one exception within the same order of magnitude. The modelled flux is, except for one outlier, always greater than the APO-derived flux.

Table of Contents

1. Introduction	5
2. Objectives and Aims.....	9
3. Methodology.....	10
3.1 Event analysis.....	13
3.1.1 Productivity-related events.....	14
3.1.2 Ventilation events.....	15
4. Results and Discussion	
4.1 Introduction.....	18
4.2 Curve fits.....	18
4.3 Seasonal cycles.....	20
4.4 Atmospheric Events.....	24
4.4.1 Seasonal distribution of atmospheric events.....	25
4.4.2 Oxidative ratios.....	27
4.4.3 Productivity events.....	28
4.4.4 Ventilation events.....	32
5. Conclusions.....	35
5.1 Summary of key findings.....	35
5.2 Limitations of the research.....	36
5.3 Suggestions for future research.....	36
6. Reference List.....	37

1. Introduction

Anthropogenic emissions of greenhouse gases are increasing and causing increasing global temperatures and climate change (IPCC, 2013). Atmospheric measurements are a vital part of observing and understanding the changes in the carbon cycle and the wider climate system and enable independent analysis of the ocean carbon cycle (Stephens et al., 1998). The ocean is the largest carbon sink (Sabine, 2004) and a vital part of the carbon cycle, however our understanding is still limited. It is therefore crucial to improve our knowledge of the ocean carbon cycle in order to understand how the ocean carbon sink may change in the future, as this will impact atmospheric CO₂ concentration as well as the marine biosphere and other ocean processes.

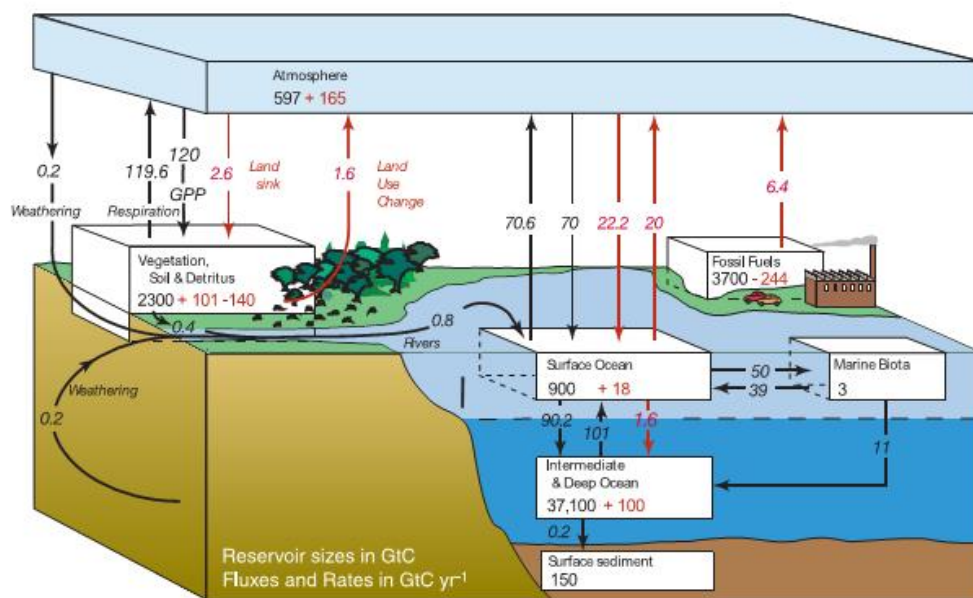


Figure 1: The Global Carbon Cycle. The black text and arrows represent the carbon cycle in equilibrium, red text and arrows represent the present carbon cycle, perturbed by anthropogenic emissions. Gt C are equivalent to Pg C. Source: IPCC, 2007.

Anthropogenic emissions of greenhouse gases are unequivocally causing rising global temperatures and global climate change. Cumulative anthropogenic CO₂ emissions between 1750 and 2011 are 555 Pg C, driving an increase of 0.85°C (1880-2012) (IPCC, 2013). These emissions are primarily from fossil fuel burning, cement making and changes in land-use. However these activities alone would cause an increase in atmospheric concentration greater than that seen from atmospheric records. This is due to the CO₂ taken up by carbon sinks (Figure 1). On the timescales of anthropogenic climate change, the terrestrial biosphere and the ocean are of greatest relevance. Figure 1 shows that anthropogenic emissions of greenhouse gases have disrupted the equilibrium of the carbon cycle and created increased uptake of CO₂ by carbon sinks (IPCC, 2007). The ocean carbon sink is especially important, as it takes up 40% of anthropogenic emissions (Sabine et al., 2004).

The ocean absorbs approximately 40% of anthropogenic CO₂ emissions (Sabine et al., 2004). This is possible due to the mixing of the surface and deep ocean and the chemical reactions that occur in the ocean. CO₂ undergoes fast hydration reactions when in the ocean and exists in equilibrium with bicarbonate and carbonate ions, which allows greater uptake of CO₂ than would be possible if all the dissolved carbon existed as CO_{2(aq)}. Biological and solubility carbon "pumps" act to transport carbon from the surface to the deep ocean, again increasing the capacity for CO₂ uptake from the atmosphere to the surface ocean. Due to carbonate chemistry, increased CO₂ absorption increases the acidity of the ocean. Ocean acidification has many negative impacts through changes in the chemical speciation and biogeochemical cycles of the ocean. Reduction of calcification of CaCO₃ shelled organisms under high CO₂ conditions are well-documented (Doney et al., 2013). This will affect a wide range of organisms, such as corals and coccolithophores, and the impacts on the broader community are still unknown. Further research into the ocean processes currently occurring is needed. It is vital that we understand the processes involved in the ocean carbon sink in order to predict how it will change in the future, as these changes could have a significant impact on the atmospheric CO₂ concentration and therefore climate change.

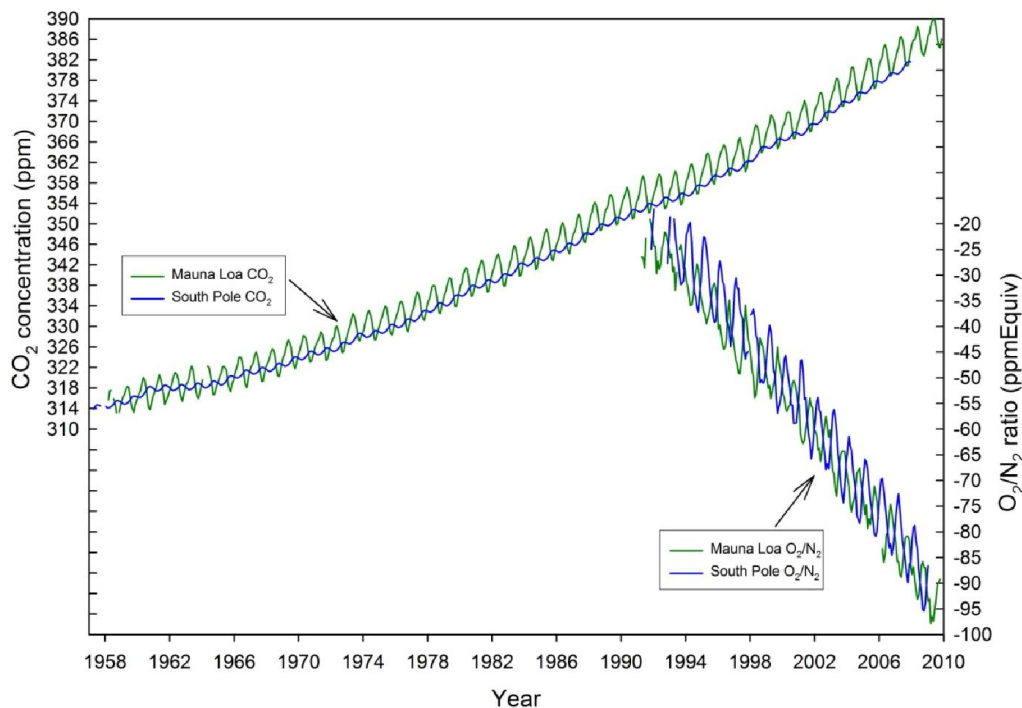


Figure 2: Atmospheric CO₂ and O₂ records from Mauna Loa, Hawaii and South Pole. Figure created from unpublished data, available at: <http://scrippsco2.ucsd.edu/>.

Atmospheric CO₂ was first measured to high precision by Charles Keeling at the Mauna Loa Observatory (Keeling, 1960). High precision atmospheric O₂ measurements were first made by Ralph Keeling in 1989. CO₂ and O₂ records from Mauna Loa, Hawaii and the South Pole Observatory are presented in Figure 2. The shows the trend of increasing CO₂ mole fraction and declining O₂, with seasonal cycles super imposed. As the CO₂ seasonal cycle is caused

by terrestrial biosphere processes, the seasonal cycle in the Southern Hemisphere is the inverse of the Northern Hemisphere. Continuous concurrent measurements of CO₂ and O₂ have been shown to be a useful tool in understanding the ocean carbon sink (Keeling and Shertz, 1992). Atmospheric O₂ measurements are challenging to make to the necessary precision. This is seen in the World Meteorological Organisation (WMO) goals for the precision of measurements: ±0.1 ppm for CO₂ and ± 2 per meg for O₂. The higher concentration of O₂ in the atmosphere, compared to CO₂, means that the changes in concentration are very small relative to the atmospheric concentration. O₂ is therefore measured as δ(O₂/N₂) with units of "per meg", where a change of 4.8 per meg of O₂ is equivalent to a 1 ppm change in CO₂. Although O₂ seasonality is mainly influenced by ocean processes due to the sea-air exchange described above, the land biosphere does affect the mole fraction. Atmospheric Potential Oxygen (APO) was therefore designed as a method to investigate the ocean fluxes of CO₂ and O₂. It is necessarily conservative with respect to the terrestrial biosphere. This is achieved using the ratio of O₂:CO₂ exchanges in terrestrial biosphere activity, which are anti-correlated. This ratio has been experimentally determined as 1.1. Using this ratio, the terrestrial biosphere exchanges can be cancelled out, leaving only the ocean effects on CO₂ and O₂ (see Equation 2 in Section 3) (Stephens et al., 1998). Except for the small long-term influence of fossil fuel emissions, APO variation is caused by O₂ fluxes due to three major processes in the ocean: biological productivity, ventilation and thermal effects. The terrestrial biosphere exchanges carbon with the atmosphere on weekly timescales, whereas atmosphere-ocean exchanges occur over yearly timescales. This is compared to the geologic carbon sink which takes centuries to exchange with the atmosphere. However ocean-atmosphere exchange of O₂ occurs over approximately three weeks (Broecker and Peng, 1982). Marine biosphere productivity takes up O₂ and releases CO₂ into the surface waters, leading to uptake of O₂ from the atmosphere and outgassing of CO₂. APO increases due to the changes in CO₂ and O₂ mole fractions. The term 'ventilation' refers to outgassing of O₂ due to mixing of deeper, oxygen-rich and carbon-depleted waters with surface waters. CO₂ is taken up from the atmosphere. APO therefore decreases. Temperature has a small effect on ocean-atmosphere fluxes of gases due to solubility changes. At higher temperatures, gas solubility in water decreases and therefore outgassing occurs. This effect contributes to the larger O₂ marine seasonality relative to CO₂ because during winter all dominant processes, including increased solubility, cause uptake of O₂ and the fluxes of CO₂ cancel out.

This method has been widely used to investigate both long- and short-term ocean fluxes. In the long term O₂ is declining due to fossil fuel burning and APO is also declining at a slower rate, partly compensated by the increase of CO₂. APO has been used in combination with other methods to quantify the ocean and terrestrial carbon sinks (Keeling and Manning, 2014). On short timescales (seasonal variation and shorter), APO variability is due to O₂ atmosphere-ocean fluxes. Short-term, quickly changing excursions from baseline atmospheric concentration are termed atmospheric 'events'. Atmospheric events can be caused by numerous processes such as deep water upwelling, phytoplankton blooms, or anthropogenic pollution. van der Laan-Luijkx et al. (2010) used continuous atmospheric measurements in the North Sea to detect a negative O₂ excursion, or atmospheric event. They correlated the

event with meteorological data and used back trajectories to confirm an ocean signal, but were unable to confidently confirm a cause for the event. van der Laan et al. (2014) used the ratio of O₂:CO₂ mole fractions during the event (oxidative ratio) to identify the cause of atmospheric events. Yamagishi et al. (2008) used continuous CO₂ and O₂ measurements from the east coast of Hokkaido island, Japan to investigate the ocean carbon cycle from April to June 2005. They found several atmospheric events characterised by periods of high APO ranging in temporal scale from hours to days. They followed a similar methodology using air mass back trajectory and monthly averaged marine NPP. In addition, they estimate the sea-air flux of O₂ using the Jacob (1999) puff model equation. This analysis assumes that all changes in the oxygen flux are due to marine productivity, without considering the impact of temperature changes. Although they look at short-term events in detail, this is only carried out over a short period (3 months). Therefore seasonal analysis of APO event variability is not undertaken. They also identify spikes in APO unrelated to NPP variability. The causes of these events are not identified.

Mace Head Atmospheric Research Station is situated on the west coast of Ireland and receives air mainly from the North Atlantic (34-51% of air (Manning et al., 2011)). Flask measurements of atmospheric CO₂ and O₂ from Mace Head have previously been compared to data from North Sea platforms and the Netherlands (van der Laan-Luijkx et al., 2010a; Sirignano et al., 2008), however continuous measurements have not yet been analysed from this site. The utility of flask data is limited and cannot reliably be used for event analysis due to the relatively low frequency of the data. The comparisons in previous analyses show a changing gradient between Mace Head and Lutjewad, the Netherlands. The CO₂ mole fraction is becoming relatively higher at Lutjewad compared to MHD and the O₂ concentration relatively lower (van der Laan et al., 2014). There has been relatively little work on constraining seasonal variability. This project will utilise a 13 month continuous dataset of atmospheric CO₂ and O₂ measurements. The higher temporal resolution provides insight into ocean processes over smaller spatial and temporal scales. This project will investigate the seasonal variability of ocean carbon cycle processes in the North Atlantic and attempt to detect and attribute causes for atmospheric events.

2. Objective and Aims

This project will investigate the spatial and temporal variability of oceanic carbon cycle processes using atmospheric CO₂ and O₂ measurements that have been collected from the Mace Head Atmospheric Research Station, Ireland. This will lead to the overall objective of using atmospheric observations to better understand ocean carbon cycle processes.

The overall objective will be achieved by carrying out the following aims:

1. Characterisation of the seasonal cycle of CO₂, O₂ and APO, using time series curve fitting programs;
2. Investigation of the contribution of ocean sources within the seasonal cycles with the aim of identifying the signals of different marine processes;
3. Detection and attribution of atmospheric 'events' that illustrate oceanic processes. This will be achieved by:
 - using air mass footprint analysis and back trajectory analysis;
 - using satellite ocean colour data to identify areas of high marine productivity
 - using mixed layer depths and dissolved oxygen concentration datasets to identify area of upwelling;
4. Calculation of the air-sea fluxes causing the atmospheric 'events' using atmospheric data from Mace Head;
5. Comparison of these fluxes to the fluxes derived from external data such as modelled Net Primary Productivity (NPP) in order to determine to what extent such datasets can be a predictor of APO and ocean carbon cycle variability.

3. Methodology

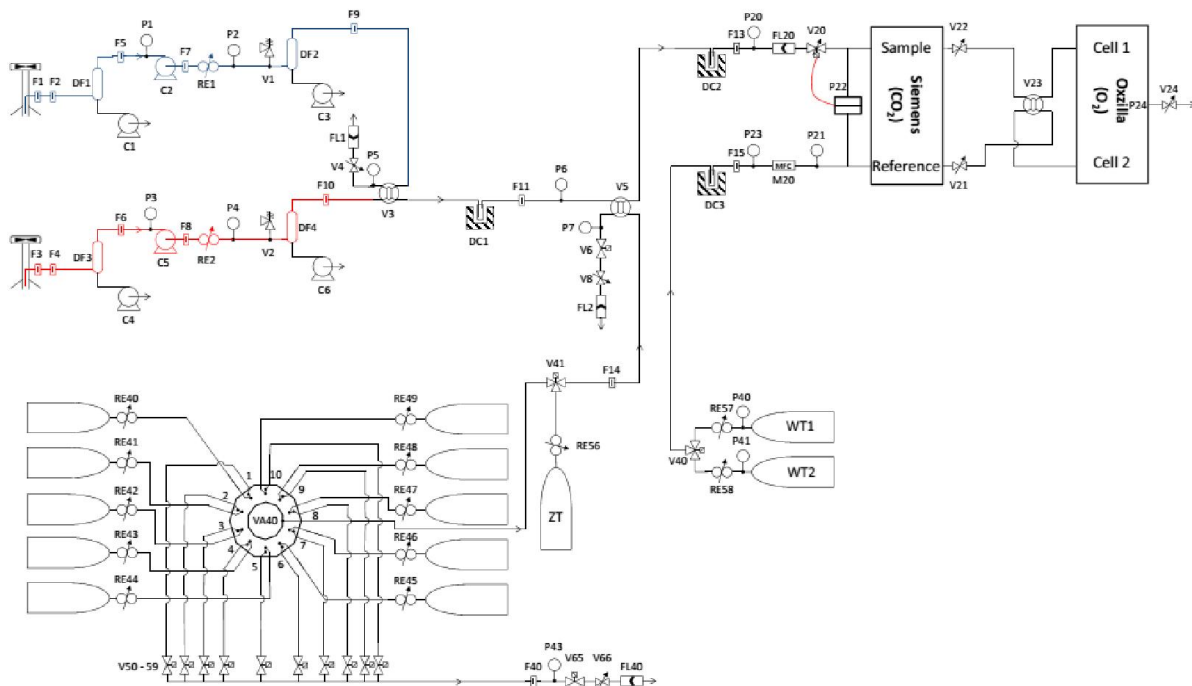
Continuous atmospheric measurements were collected from the Mace Head Atmospheric



Figure 3: Map showing the location of Mace Head Atmospheric Observatory (Google, 2009; GeoBasis-DE/BKG, 2015).

Observatory, situated on the west coast of Ireland (53° 20' N, 9° 54' W) (Figure 3). The gas handling system is shown in Figure 4. Air is sampled from two intakes and dried using two water traps. The system is maintained at a constant temperature and pressure. The CO₂ analyser used is the Siemens Ultramat 6E analyser and a Sable Systems Oxzilla II is used to measure O₂. Extensive diagnostic data is collected throughout the system including temperatures, pressures and flow. The system is calibrated against three calibration cylinders with known concentrations of CO₂ and O₂. CO₂ measurements are referenced to the WMO X2007 scale.

Figure 4: gas handling diagram of the atmospheric CO₂ and O₂ measuring system at Mace Head showing



the two air inlets (blue and red lines), water traps (DC1, DC2, DC3, DF1 and DF3), analysers and calibration gases (ZT, WT). P indicates a pressure transducer, F indicates a flow meter, V a valve and RE a regulator.

Atmospheric O₂ is measured as the $\delta(O_2/N_2)$ ratio with units of "per meg", using the Equation 1:

$$\delta(O_2/N_2) = ((O_2/N_2)_{\text{sample}} / (O_2/N_2)_{\text{reference}}) - 1 \quad (\text{Equation 1})$$

The equation assumes N₂ to be constant as it has a very high abundance in the atmosphere and is stable, with relatively small fluxes. We report O₂ using this method because changes in the concentration of trace gases such as CO₂ will affect the mole fraction of O₂, possibly leading to erroneous conclusions about O₂ fluxes because of observed changes in the O₂ mole fraction. A 1 ppm change in CO₂ mole fraction is equivalent to a 4.8 per meg change in O₂ (Keeling and Manning, 2014). At Mace Head, O₂ measurements are referenced to the Scripps Oxygen scale.

APO is calculated using Equation 2:

$$\delta APO = \delta \left(\frac{O_2}{N_2} \right) + 1.1 \times (X_{CO_2} - 350) / 0.2094 \quad (\text{Equation 2})$$

where 1.1 is the O₂:C molar exchange ratio for the land biosphere; X_{CO₂} is the CO₂ mole fraction in dry air in ppm; 350 is an arbitrary value, and 0.2094 is the conversion factor for mole fraction to per meg units (Stephens et al., 1998). As discussed in the Introduction, APO is designed to be conservative with respect to the terrestrial biosphere through the use of the molar exchange ratio. The calculation of APO therefore enables us to determine the spatial and temporal patterns of air-sea fluxes of O₂ and CO₂ (Stephens et al., 1998).

The atmospheric data were flagged to remove bad air sample data. I used weekly, daily and hourly plots of CO₂, O₂ and APO and diagnostic data of the raw two-minute averages produced from an Interactive Data Language (IDL) program written by my supervisor Andrew Manning. These plots were examined visually and against diagnostic and calibration data. In some cases where bad calibrations had occurred, I was able to recover data by adjusting the data based on information recorded during calibrations. Once all the data was quality checked I applied the flags to the data using a R script written by Penelope Pickers. I made a number of modifications to the script to fit my dataset. I also wrote some R code to produce *.csv files of the two-minute data and hourly averages of the flagged data.

In order to separate out the seasonal cycle from the data, the baseline (unpolluted) data must be defined. Two methods were used to identify the baseline data in order to improve the robustness of the results. The first method used was statistical and utilised a script written by Penelope Pickers. Firstly the "rfbaseline" function from the IDPmisc package (Locher et al., 2012) in R is used to calculate the statistical baseline of the data. This method is also known as robust extraction of baseline signal (REBS) and was developed by Ruckstuhl et al. (2001, 2012). The advantage of this method is that it is non-parametric and uses an asymmetric distribution of the residuals of the LOESS (Locally Weighted Scatterplot Smoothing) fit. As a result the baseline is not biased by large pollution spikes occurring in one direction. Using this function, residuals of the baseline are calculated and the data are flagged if the residuals are a certain number of standard deviations away from the calculated baseline.

The second method is based on meteorological data. I used hourly averaged meteorological data collected at Mace Head and provided to me by Michel Ramonet (Laboratoire des Sciences du Climat et de l'Environnement (LSCE), France). I wrote an R script to read in the

meteorological data, combine it with the hourly averaged atmospheric measurements and split the data into 'baseline' or 'polluted' based on wind speed and direction. I used the Bousquet et al. (1996) restricted baseline conditions which have been used in several atmospheric studies of Mace Head data (Derwent et al., 2002; Sirignano et al., 2010; van der Laan-Luijkx et al., 2010). Data were defined as 'baseline' if the wind direction was between 210° and 290° and the wind speed was over 4 m s⁻¹ or if the wind direction was between 200° and 300° and the wind speed was over 8 m s⁻¹ (Bousquet et al., 1996).

Hourly averaged baseline data were then used for time series decomposition. This process separates out the long-term trend, the seasonal cycle, and any irregular variations in the timeseries. As demonstrated by Pickers and Manning (2015), it is important to use more than one curve fitting method in order to eliminate possible bias. I used three methods; STL (Seasonal Trend decomposition using LOESS), CCGCRV (Carbon Cycle Group CuRvE) and HPspline (Harmonic, Polynomial, spline). STL is a moving average technique with an inner and an outer loop which runs iteratively until the approximations of the trend and seasonal components converge (Cleveland et al., 1990). HPspline is a parametric curve-fitting program written in Fortran. It involves three routines in Numeric Recipes in Fortran (Press et al., 1996) and involves fitting data to a harmonic function, a polynomial equation and a stiff cubic spline (Reinsch, 1967). HPspline was run with two harmonics because my dataset is relatively short. CCGCRV is a digital filtering curve fitting program written in IDL. It fits a polynomial equation combined with a harmonic function and then filter the residuals using a Fast Fourier Transform (FFT) (Thoning et al., 1989). Further details on all three curve-fitting programs can be found in Pickers and Manning (2015). Three years of data were required for STL and CCGCRV to produce output and so I also used three years data for HPspline for consistency. This was achieved by generating artificial data for calendar years 2013 and 2015 by using the long term trend observed at Weybourne, Norfolk, as this station is close in location, and similarly situated on the coast (Wilson, 2013). I ran STL in R, using a script written by Zoe Fleming (National Institute of Water and Atmospheric Research (NIWA)) and Penelope Pickers. In order to run STL the data had to be interpolated as the version in R cannot run on unevenly spaced data. This was achieved using an R script. Penelope Pickers kindly ran CCGCRV and HPspline on my data for me. The decomposition of the timeseries produces a trend, the detrended seasonal cycle and residuals. The curve fit is the trend plus the detrended seasonal cycle. I calculated the seasonal cycle amplitudes from the detrended seasonal cycle.

For all events the oxidative ratio was calculated. This is the molar ratio of O₂:CO₂ during the event. The ratio can be used to characterise the carbon cycle process that caused the event, for example fossil fuel burning has a global average ratio of 1.4, although different fuels have different ratios due to their chemical composition (van der Laan et al., 2014). The oxidative ratio can be calculated by plotting the two minute data of CO₂ and O₂ concentrations against each other and calculating the least squares linear regression. The ratio is the slope of the line.

3.1 Event analysis

I detected events visually based on the CO₂, O₂ and APO mole fractions. As this project is focussed on ocean carbon cycle processes, I only selected events with APO excursions. For each event I produced plots of O₂ against CO₂ in R and calculated the regression line.

To analyse atmospheric events I carried out air mass back trajectory analysis to determine where each air mass had travelled from before arriving at Mace Head. HYSPLIT (Hybrid Single-Particle Lagrangian Integrated Trajectory) produces back trajectories for air particles using existing meteorological data (Draxler and Hess, 1998). This is a simple Lagrangian atmospheric transport model and does not include factors such as turbulence (Fleming et al., 2012). HYSPLIT is available to run online (http://ready.arl.noaa.gov/HYSPLIT_traj.php) and takes only a few minutes to run. I therefore used this for the initial check, and also for the majority of my event analysis. For a few of the most interesting events, the Met Office's Numerical Atmospheric Dispersion Modelling Environment (NAME) was used (Jones et al., 2007; Ryall and Maryon, 1998). NAME is a Lagrangian Particle Dispersion Model that is driven by 3D meteorological data. In contrast to simpler models atmospheric turbulence is included in the simulation by using a random walk technique (Manning et al., 2011).

10,000 inert trace particles are released at each three hourly interval and NAME produces an integration of the number of particles per grid cell over the duration of the run (Fleming et al., 2012). The UEA supercomputer has NAME functionality and Penelope Pickers ran NAME to produce footprints. An example is shown in Figure 5. NAME was run in backwards mode for three days at three-hour intervals for the day of the event and the days preceding and following the event. This provides context for the event. The resolution is 0.25° latitude by 0.25° longitude. Events that showed a terrestrial origin were removed from further analysis.

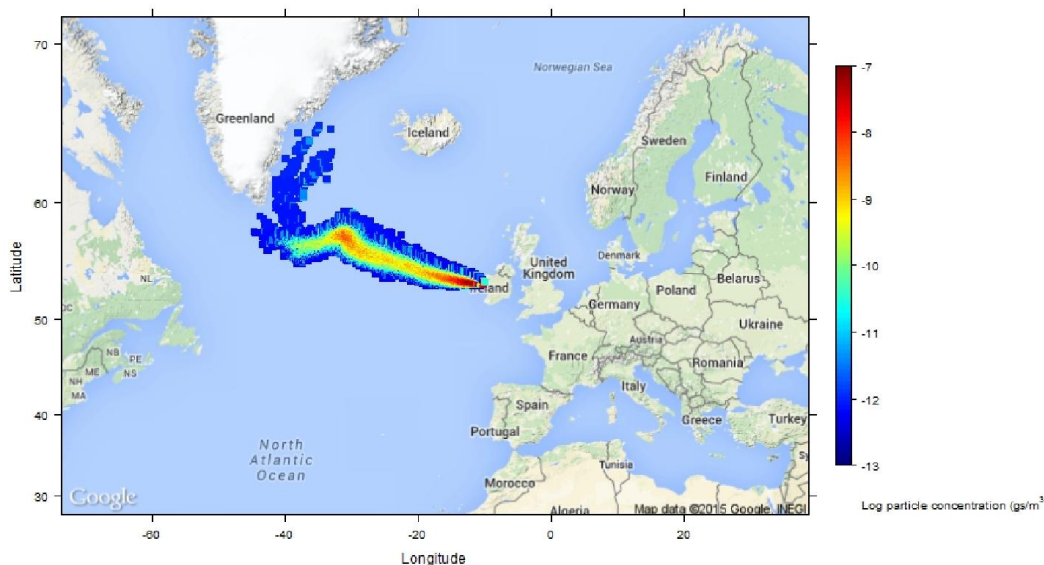


Figure 5: a NAME air mass footprint showing the origins of the air arriving at Mace Head on 01 June.

3.1.1 Productivity-related events

Marine productivity is the most likely cause of positive APO excursions above the baseline. In order to detect productivity related events I used MODIS (Moderate Resolution Imaging Spectroradiometer) Aqua ocean colour data which is available from Oregon State University and can be used to derive estimates of primary productivity (OSU, 2014). Ocean colour can be used as a proxy for the amount of chlorophyll-*a* in the surface waters. Modelling is required to obtain information about sub-surface waters and productivity estimates. I used eight-day average Net Primary Productivity (NPP) datasets (Figure 6) modelled from satellite data using the Vertically Generated Production Model (VGPM) (Behrenfeld and Falkowski, 1997), which is a commonly used productivity model. The spatial resolution is 0.2° latitude by 0.2° longitude (OSU, 2014).

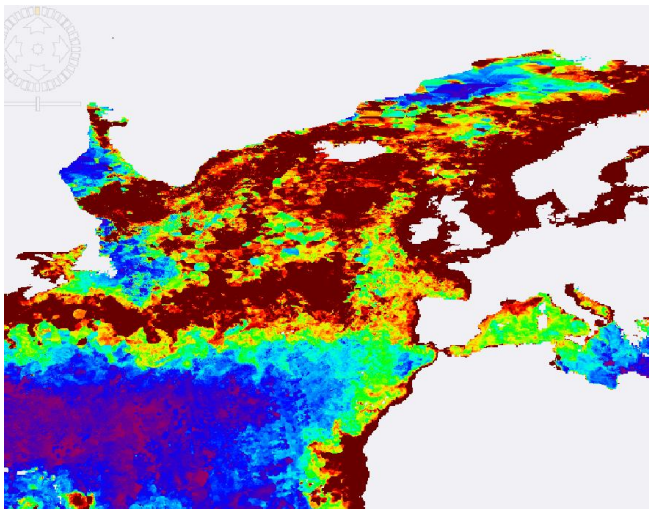


Figure 6: NPP derived from ocean colour satellite data modelled with the VGPM for 25/05/2014 to 01/06/2014

To combine the air mass back trajectories and the NPP images I used a piece of software called SeaDAS available from the National Oceanic and Atmospheric Administration, USA (NOAA) (<http://seadas.gsfc.nasa.gov/installers/>). I used this software to overlay the back trajectories onto the NPP images and calculate the mass flux, similar to the method used by Barningham (2013). I followed a version of the Yamagishi et al. (2008) method of estimating the NPP from the satellite image. Yamagishi et al. (2008) took the difference between the bloom NPP and the surrounding NPP i.e. the change in NPP, to be comparable to the change in observed APO at the station. This is difficult to keep consistent and also not possible to calculate for a wider area in SeaDAS. So as an approximation of this method I took the difference between the maximum NPP and the mean NPP within the back trajectory area. Any events that did not correlate with an area of relatively higher productivity were removed from further analysis.

To calculate the air-sea flux required to produce the APO change observed at Mace Head during events I used the Jacob (1999) ‘Puff’ model (Equation 3). This can be used to calculate the flux of a gas into a moving column of air (in $\text{mol m}^{-2} \text{yr}^{-1}$), and has been used in multiple studies (Lueker, 2004; Thompson et al., 2007; Yamagishi et al., 2008) to calculate air-sea flux of O_2 :

$$Flux = \frac{\Delta C \cdot h}{t[1 - \exp(-L/ut)]} \quad (\text{Equation 3})$$

where ΔC is the change in atmospheric concentration within the column (in mol m⁻³), h is the vertical mixing height obtained from HYSPLIT (<http://ready.arl.noaa.gov/READYamet.php>) (in metres), L is the wind fetch estimated by importing the HYSPLIT trajectory into Google Earth and measuring using the measuring tool (in metres), u is the average wind speed within the back trajectory area obtained from the NOAA sea winds dataset (<https://www.ncdc.noaa.gov/data-access/marineocean-data/blended-global/blended-sea-winds>, Zhang et al., 2006a; Zhang et al., 2006b) (in m yr⁻¹) and t is an e -folding lifetime representing atmospheric mixing within the column (in years). t is calculated using Equation 4:

$$t = \frac{\Delta C/e}{\Delta C/t_e} \quad (\text{Equation 4})$$

where t_e is the duration of the event.

Equation 3 gives the flux in mol m⁻² yr⁻¹. I used the O₂:C exchange ratio of 1.4 (Laws, 1991) and assumed steady state conditions for the net community productivity to convert the flux into units comparable with the ocean colour data (mg C m⁻² day⁻¹).

I also investigated the relationship between the flux as calculated above and the O₂ flux calculated from ocean heat fluxes. The NEMO (Nucleus for European Modelling of the Ocean) PlankTOM (Plankton Types Ocean Model) model produces heat fluxes and oxygen fluxes from the ocean (Blaine, 2005). Pickers et al. (2015) used the NEMO PlankTOM model coupled with NAME to produce modelled changes in APO and investigated whether this model captured observed negative excursions in APO. The data are at a daily resolution and a spatial resolution of 2° by 2°. These data were provided by Corinne Le Quéré (Tyndall Centre, UEA).

3.1.2 Ventilation events

Negative APO excursions from the baseline are most likely due to ventilation or upwelling events which are indicated by a deeper ocean mixed layer. I followed the Barningham (2013) method to design a conceptual model to investigate these events. I used mixed layer depth (MLD) data obtained from Argo floats (<http://www.Argo.ucsd.edu/>), and the change in dissolved oxygen concentration to calculate an air-sea flux. Argo floats produce depth profiles of variables including temperature, salinity and pressure. The accuracies of the temperature, salinity, and pressure sensors on the Argo floats are ±0.005°C, ±0.01 psu, and ±2.4 dbar, respectively (Argo Science Team, 2001). The floats sink to a set parking depth and then float freely. Every ten days the floats ascend to the surface, measuring continuously. These measurements are transmitted via satellites and are available, averaged to standard

depth levels (Dong et al., 2008). The MLD is calculated using potential density and potential temperature. I used the Hosada et al. (2010) data of MLD, temperature and salinity (www.jamstec.go.jp/e). The dataset comprises high quality Argo float data at 2° by 2° spatial resolution. MLD is calculated using the threshold difference method. They provide two datasets: one with the MLD calculated using temperature, and the other using salinity. In both cases they assume a shallow iso-thermal or iso-pycnal layer respectively and use the finite difference method to calculate this (Hosada et al., 2010). Using these data I found the mean and maximum MLD within the area of influence from the HYSPLIT back trajectory, using the SeaDAS software package. Any events with a shallow mixed layer (50m or less) were removed from analysis.

I then used dissolved O₂ data from the World Ocean Database (<https://www.nodc.noaa.gov/OC5/WOD13>) to see if the APO-derived flux was possible or likely to occur in the area of influence. I used the software package Ocean Data View (ODV) to view the files. ODV is available from the Alfred Wegner Institute (<http://odv.awi.de>) and is designed specifically for oceanographic datasets. I used two complementary methods of calculating the ΔpO₂. Firstly I used PFL (profiling floats) data and found floats that were within the area of influence during the duration of the back trajectory. I calculated the change in pO₂ between the MLD (as determined above) and the surface for all floats. When determining which floats to use, I considered the position of the air mass over time during the duration of the back trajectory. The second method to calculate the ΔpO₂ utilised monthly mean pO₂ from the World Ocean Atlas 2013 (<https://www.nodc.noaa.gov/OC5/woa13/woa13data.html>). These are data from different sources averaged together at standard depths. I calculated the ΔpO₂ as the change in pO₂ between the MLD and the surface. I chose to use these two methods because the PFL data is real time data and therefore should give a more realistic picture for short-term events, however the coverage is very sparse and therefore the results are less reliable. The average monthly dataset incorporates a large amount of data and is interpolated to provide full ocean coverage, however it is a climatology and therefore has limited use when considering short term atmospheric events.

I then used the calculated change in dissolved O₂ concentration to calculate the air-sea flux that would result. I used the following equation from Garcia and Keeling (2001) and Wanninkhof (1992):

$$Flux = \rho \cdot k_{O_2} \cdot \Delta[O_2] \quad (\text{Equation 5})$$

where ρ is the density of the seawater (g cm⁻³) (I chose to use the mean density of seawater, 1.025 g cm⁻³), Δ[O₂] is the oxygen anomaly (mol m⁻³), and k_{O₂} is the gas transfer velocity for O₂ (m yr⁻¹), which is calculated using Equation 6, from Wanninkhof (1992):

$$k_{O_2} = 0.39u^2 \left(\frac{Sc_{O_2}}{660} \right)^{-\frac{1}{2}} \quad (\text{Equation 6})$$

where u is the wind speed in m yr^{-1} and Sc_{O_2} is the Schmidt number for O_2 . I calculated Sc_{O_2} using Equation 7 from (Wanninkhof, 1992):

$$Sc_{O_2} = 1953.4 - 128T + 3.9918T^2 - 0.05009T^3 \quad (\text{Equation 7})$$

where T is sea surface temperature (SST) in $^{\circ}\text{C}$. The oxygen anomaly, $\Delta[O_2]$, from Equation 5 is calculated using Equation 8, from Garcia and Keeling (2001):

$$\Delta[O_2] = [O_2] - [O_2]^* + \delta_{skin} \quad (\text{Equation 8})$$

where $[O_2]$ is the measured dissolved O_2 concentration of the sea water calculated from Argo data as described above, $[O_2]^*$ is the O_2 solubility, and δ_{skin} is the skin temperature correction. The value of δ_{skin} is in general very small (about $\pm 0.001 \text{ mol m}^{-3}$), therefore I have not applied this correction. $[O_2]^*$ is calculated using Equation 9 from Garcia and Gordon (1992):

$$\ln[O_2]^* = A_0 + A_1T_s + A_2T_s^2 + A_3T_s^2 + A_3T_s^3 + A_4T_s^4 + A_5T_s^5 + S(B_0 + B_1T_s + B_2T_s^2 + B_3T_s^3) + C_0S^2 \quad (\text{Equation 9})$$

where S is salinity in psu, and A_0 to A_5 , B_0 to B_3 and C_0 are constants from Garcia and Gordon (1992).

T_s is given by Equation 10, also from Garcia and Gordon (1992):

$$T_s = \ln [(298.15 - t)(273.15 + t)^{-1}] \quad (\text{Equation 10})$$

where t is the seawater temperature in $^{\circ}\text{C}$.

Equation 5 produces an air-sea flux value that can be compared to the APO-derived flux value.

The temperature, salinity and density values used in Equations 5 to 10 are taken from the MLD dataset based on Argo floats from Hosada et al. (2010) available at www.jamstec.go.jp/e. I used averages within the back trajectory area, calculated by importing the NetCDF files into SeaDAS and overlaying the back trajectory. I calculated the APO-derived flux following the same method as above.

4. Results and Discussion

4.1 Introduction

In this section I will present my results and discuss wider ocean carbon cycle relevance, and relevance to the literature. The hourly averaged data are plotted in Figure 7. The standard deviations of the two minute averaged data and of the calibrations provide an indication of error (Table 1). O₂ is clearly more variable than CO₂.

	Two-minute averaged data	Target Tank Calibrations	Zero Tank Calibrations
CO ₂ (ppm)	0.034753	0.06296	0.08585
O ₂ (per meg)	14.005	7.926	7.569

Table 1: standard deviations of the raw data, and two calibration readings. (APO is a calculated variable and therefore not included).

This section will present results and discuss the curve fits and baseline data, the detrended seasonal cycles of CO₂, O₂ and APO, atmospheric event characteristics, and evaluate the conceptual models for both productivity and ventilation events.

4.2 Curve fits

The hourly averages were plotted against all three curve fits. The results are similar overall. CCGCRV appears to be more sensitive to short-term variability. STL has several anomalies which may be due to the use of lower frequency data (weekly/monthly) as this program does not run well on high frequency data. The curves produced do not fit along the bottom (for CO₂) or top (for O₂ and APO) of the data as would be ideal. For the statistically derived baseline, the rfbaseline function did not fit perfectly along the bottom (top) for the full data; for CO₂ (O₂ and APO) it always fits slightly below the bottom of the data in the spring and above in the autumn/winter. This led to issues with choosing the standard deviations used in the second part of the baseline process. A compromise had to be taken between flagging actual baseline data as polluted during the spring and leaving polluted data within the baseline data in the autumn. This means that the baseline data used to produce the curve fits is not an entirely accurate representation of the baseline observations at Mace Head, and the curve fits appear slightly polluted. However, this problem is also present in the curve fits based on meteorological baselines, which does not involve the use of the rfbaseline function. Therefore there is a wider problem with the curve fits. In the future I would look into this problem in more depth and produce a more accurate baseline.

Another limitation or source of error within the baseline and curve fitting procedure is the value used to force a trend in the duplicated data. This value was taken from a previous study using Weybourne data, due to the similar latitude and coastal location. However Weybourne does receive slightly more terrestrial air masses due its location and therefore the log-term trend at Weybourne could be higher than the actual trend at Mace Head. Despite the trend of 2.41 ppm for CO₂ forced through the duplicated data, the average trend calculated by the curve fitting programs is 2.11 ppm. For O₂, a trend of -25.3 per meg was applied to the duplicated data, compared to an average of -23.98 per meg produced by the curve-fitting programs. This suggests that the real trend within the data is smaller than the trend forced. Although I am not analysing the trend due to the short term dataset, this could impact the curve fits.

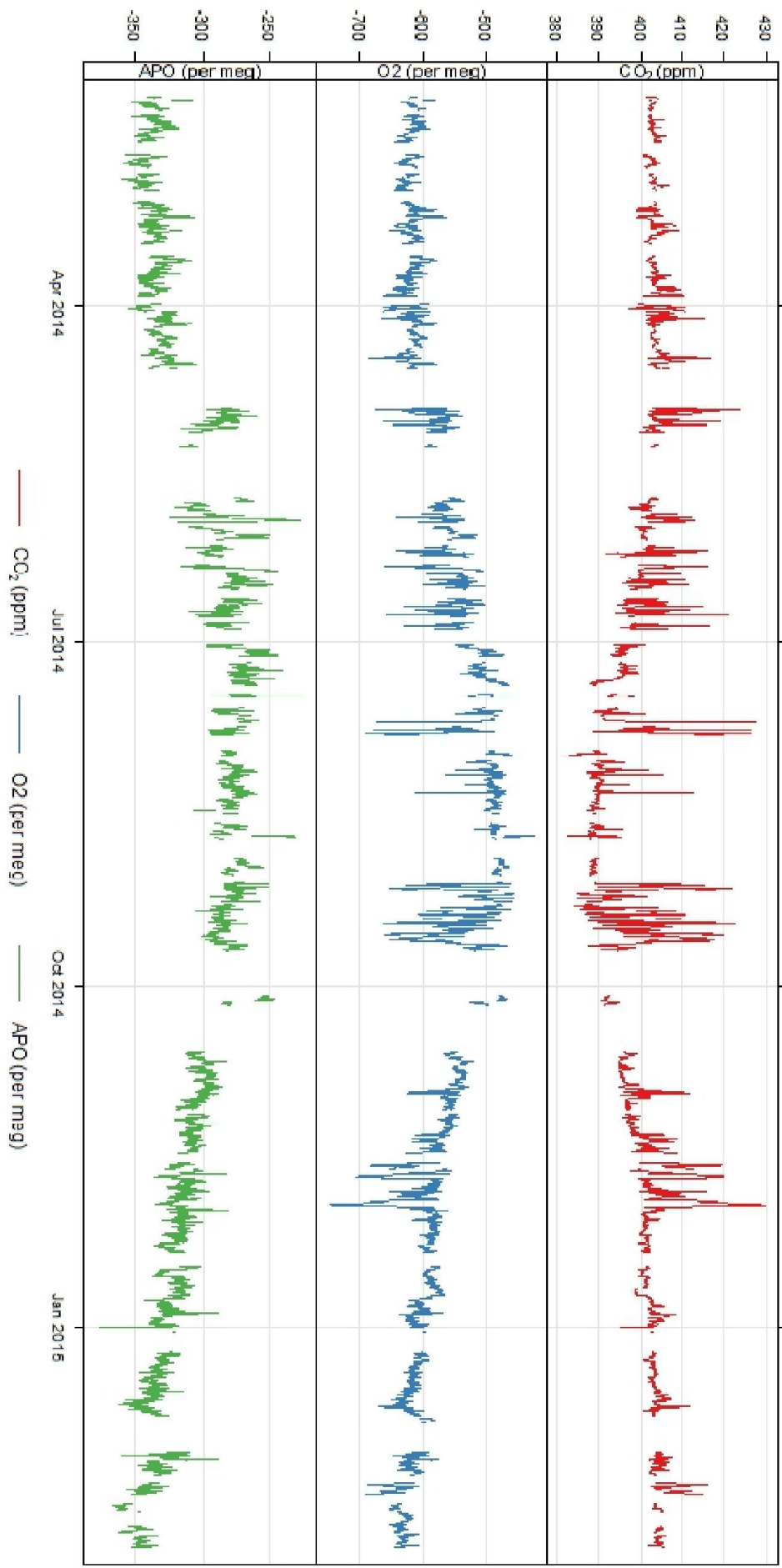
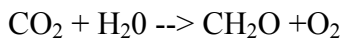


Figure 7: Hourly averaged CO₂, O₂ and APO atmospheric measurements from Mace Head.

4.3 Seasonal cycles

Figures 9, 10 and 11 show the detrended seasonal cycles derived from the statistical baselines for CO₂, O₂ and APO. CO₂ and O₂ are clearly inversely correlated as is expected. The CO₂ seasonal cycle has a minimum in August and a maximum in April. The timing correlates well with previous studies using flask measurements at Mace Head (Sirignano et al., 2010; van der Laan-Luijkx et al., 2010). The shape of the STL seasonal cycle is anomalous, although the timing of the maximum and minimum is not greatly affected. HPspline produces the smoothest curve, and is most similar to the seasonal cycle produced by van der Laan-Luijkx et al. (2010), potentially due to similar curve-fitting methods. The shape and timing of the seasonal cycle is due to processes in the terrestrial biosphere. In the summer, solar insolation is stronger and photosynthesis dominates the terrestrial biosphere. Photosynthesis requires CO₂ and produces O₂:



Convective mixing of the atmosphere is also stronger because the PBL is higher. These factors combine to cause a lower CO₂ mole fraction during the summer. In the autumn and winter solar radiation is weaker and respiration dominates. The PBL is lower and mixing is weak and infrequent. The CO₂ mole fraction therefore reaches its peak. A similar cycle occurs diurnally, especially during the summer when the PBL is more variable.

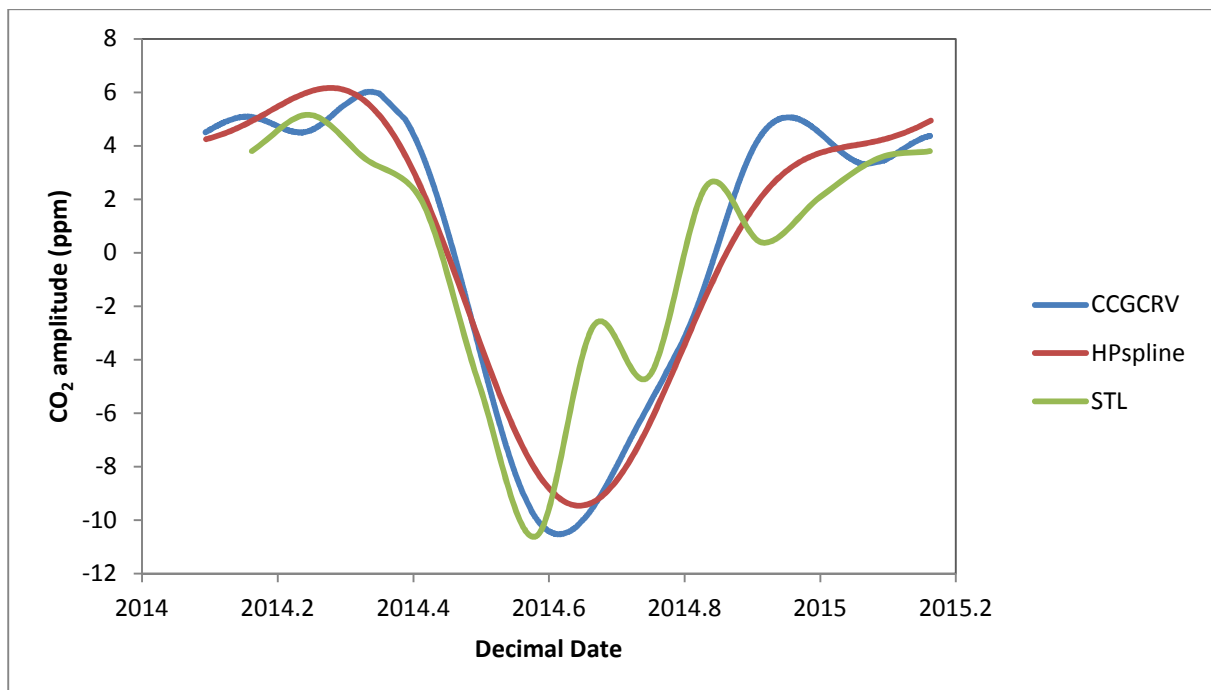


Figure 9: Detrended seasonal cycle of CO₂ produced by CCGCRV, HPspline and STL for the statistical baseline.

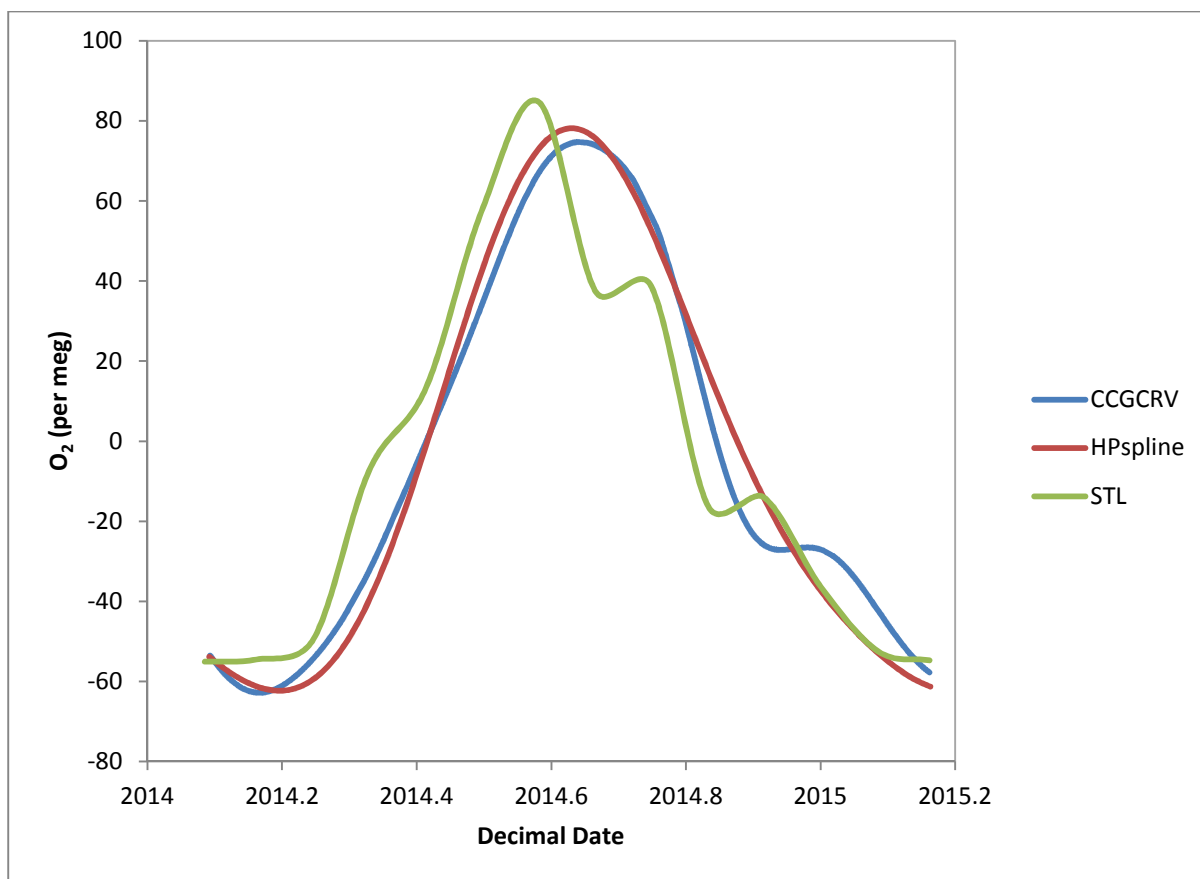


Figure 10: The detrended seasonal cycle of O₂ produced by CCGCRV, HPspline and STL for the statistical baseline.

The O₂ minimum occurs in March, slightly earlier than the absolute peak in CO₂ values, and the maximum occurs in August, correlating well with the CO₂ minimum (Figure 9). This timing is the same as the results from Sirignano et al. (2010), however van der Laan-Luijkx et al. (2010) find an earlier minimum during February. The STL seasonal cycle has similar anomalies to the CO₂ seasonal cycle and HPspline is again the smoothest curve. The CCGCRV seasonal cycle has an unusually abrupt peak.

O₂ seasonality is primarily controlled by the ocean because all the ocean processes reinforce each other in one season. However, the terrestrial biosphere also has an effect, as the processes discussed above have an inverse effect on the O₂ concentration. There are also small effects from fossil fuel burning seasonality, atmospheric transport, wind speed (which influences the air-sea gas exchange) and the supply of productivity-limiting nutrients. There are three ocean processes that influence O₂: productivity, ocean upwelling or ventilation, and temperature. Respiration, which requires O₂, is dominant in the marine biosphere during the winter resulting in greater uptake of O₂. Ocean mixing during the winter mixes O₂-poor subsurface waters with surface waters, leading to uptake of O₂ from the atmosphere. Surface waters are colder and therefore more highly soluble for gases; this also creates more uptake of O₂. During the summer these processes reverse: stratified waters prevent mixing and create a higher pO₂ in the surface waters; warmer waters are less soluble; and photosynthesis produces O₂ in the surface waters further increasing the pO₂.

The APO meteorologically-derived baseline appears polluted, and therefore I have chosen to use only the statistically-derived seasonal cycles (Figure 11). The detrended seasonal cycles produced by HPspline and STL are quite similar with maxima in July and minima in

February. The CCGCRV seasonal cycle has less of a smooth curve, with a secondary peak in June before the maximum in September. The minimum occurs in February, as in HPspline and STL. As APO is designed to be conservative to the terrestrial biosphere, the seasonal cycle reflects the seasonal cycle of ocean carbon cycle processes. On seasonal timescale, these processes have a greater impact on the atmospheric O₂ mole fraction and therefore the APO seasonal cycle is quite similar to the O₂ seasonal cycle. The maximum in July reflects marine productivity and the minimum in February reflects greater mixing and uptake of O₂. Subduction of surface waters also occurs during the winter, in the north-east Atlantic, and may also contribute to the seasonal cycle (Karleskind et al., 2011).

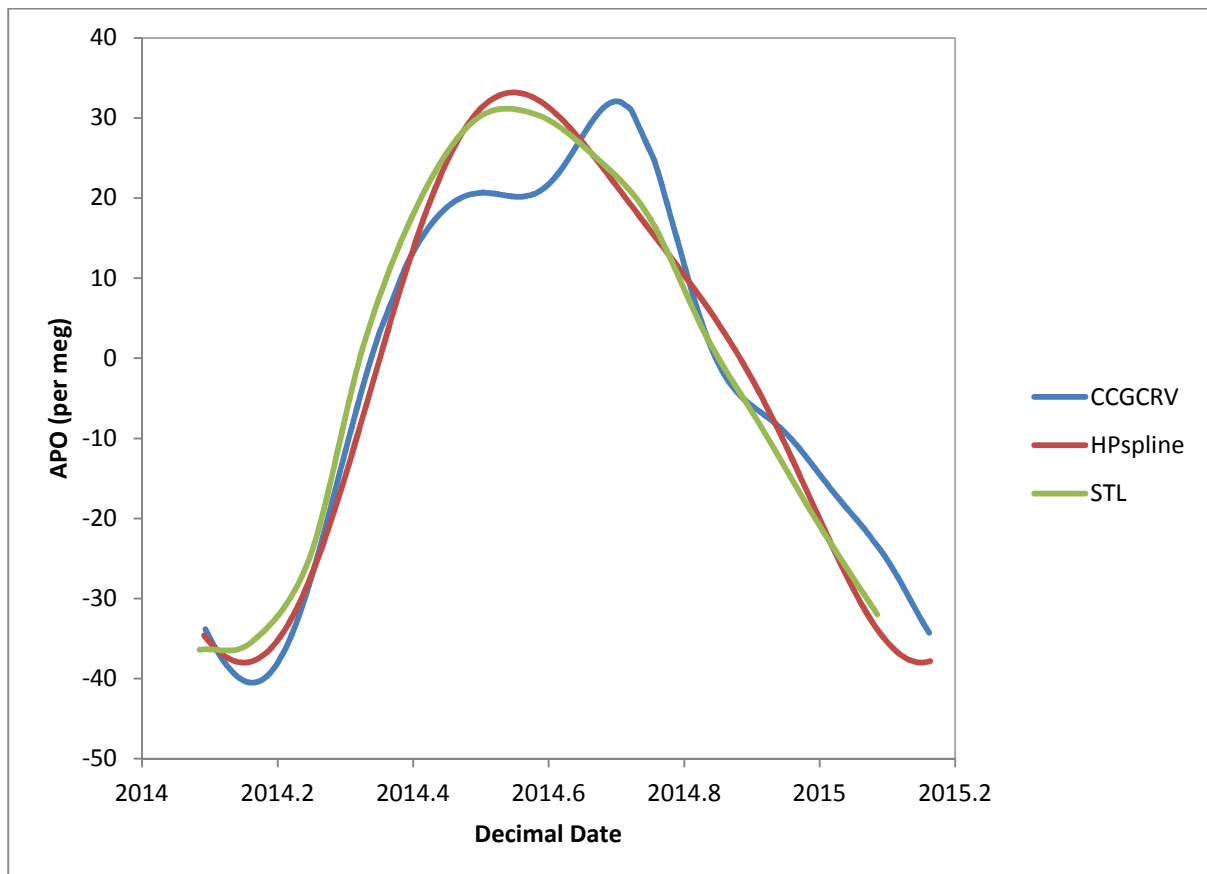


Figure 11: The detrended seasonal cycle of APO produced by CCGCRV, HPspline and STL for the statistical baseline.

van der Laan-Luijkx et al. (2010) find a secondary peak in the APO seasonal cycle which is very similar to the CCGCRV seasonal cycle. Neither STL or HPspline cycles show this feature. The curve-fitting technique used by van der Laan-Luijkx et al. (2010) is a combination of three-harmonics and a linear trend.

I calculated the seasonal peak-to-trough amplitudes of the detrended seasonal cycles (maximum seasonal value minus the minimum seasonal value). As I have six curve-fits, three from statistical-derived baselines and three from meteorological-derived baselines, I calculated the standard deviation of the six values (Table 2). The seasonal amplitude of APO is slightly over half the seasonal amplitude of O₂. This agrees with previous findings from Mace Head data (van der Laan-Luijkx et al., 2010).

	CO ₂ amplitude (ppm)		O ₂ amplitude (per meg)		APO amplitude (per meg)	
	Statistically derived baseline	Meteorological derived baseline	Statistically derived baseline	Meteorological derived baseline	Statistically derived baseline	Meteorological derived baseline
CCGC RV	18.7	20.2	145.6	157.6	77.9	77.1
Hpspline	15.6	16.0	140.4	143.8	71.2	74.7
STL	15.8	20.4	141.2	165.2	69.4	89.1
Mean	16.7 (±1.73)	18.9 (±2.47)	142.4 (±2.78)	155.6 (±10.8)	72.8 (±4.51)	80.3 (±7.71)
Overall Mean	17.783 (±2.25)		148.9667 (±10.1)		76.5667 (±6.97)	

Table 2: The seasonal cycle amplitudes of CO₂, O₂ and APO calculated from the detrended seasonal cycles produced by three different curve fitting programs and using two baseline datasets.

CCGCRV produces the largest seasonal amplitudes for all species when using the statistical baselines, however when using meteorological-derived baselines STL produces the largest seasonal amplitudes, again across all species. This suggests that the two methods of defining the baseline produce data with features more likely to be emphasised by one curve fitting program. The meteorological-derived seasonal amplitudes have a larger standard deviation. Fang et al. (2015) suggest that meteorological methods to determine the baseline are best. However they use a more complex method involving daytime data only to compensate for the effect of the varying height of the PBL, in addition to wind direction and wind speed. They also use data from an inland station in their study, and as Mace Head is a coastal station there are different factors to consider.

Station	Mace Head (van der Laan-Luijkx et al., 2010)	Shetland Islands (Kozlova et al., 2008)	Weybourne, Norfolk (Wilson, 2013)	F3 North Sea Oil Platform (van der Laan-Luijkx et al., 2010)	Lutjewad, Netherlands (van der Laan-Luijkx et al., 2010)	Ochsenkopf, Germany (Thompson et al., 2009)
Location	53.33°N, 9.9°E	60.28°N, 1.28°W	52.95°N, 1.12°E	54.85°N, 4.73°E	53.4°N, 6.35°E	50.03°N, 11.8°E
Period	1998-2009	2004-2008	2009-2012	2006-2009	2000-2009	2006-2008
CO ₂ amplitude (ppm)	14.0 ±0.3	15.4	14.9 ±0.8	15.2 ±0.1	12.0 ±0.6	15.46 ±1.04
O ₂ amplitude (per meg)	142 ±6	163	134.2 ±7.8	144 ±2	114 ±8	134.6 ±6.8
APO amplitude (per meg)	74 ±6	95	59.0 ±5.6	111 ±2	64 ±6	43.1 ±3.3

Table 3: Summary of seasonal cycle amplitudes of CO₂, O₂ and APO for north-western European stations of similar latitudes. After Wilson, 2013.

I compared the seasonal amplitudes with a range of datasets from north-western Europe from Wilson (2013) (Table 3). I found that the CO₂ seasonal amplitude is larger than in previous data from Mace Head, and larger than in all the data collected by Wilson (2013) including the continental site of Ochsenkopf, Germany. This is unexpected as continental sites are influenced more by the land biosphere, which is the main driver of CO₂ seasonality. However, the Ochsenkopf average is based on only a three year timeseries and therefore is less reliable than other data compared to. The standard deviation is an order of magnitude higher than these. van der Laan (2014) found a changing gradient between Mace Head and Lutjewad, Netherlands. CO₂ is increasing in Lutjewad relative to Mace Head, and this may be impacting the seasonal amplitude.

The O₂ seasonal amplitudes derived from statistical baselines are similar to the previous MHD value, and the value at the F3 oil platform which is also a very ocean influenced station. The seasonal amplitudes from the meteorological baseline are all larger, approaching the value at the Shetland islands, which is more influenced by the ocean. The mean seasonal amplitude is slightly larger than the amplitude at the F3 oil platform. The standard deviation is similar to the data from Wilson (2013).

The APO seasonal amplitude from statistical baselines is similar to the previous Mace Head value, though slightly lower, perhaps suggesting that there is slightly less ocean variability during 2014-2015 compared to the average over 1998-2009. The meteorologically-derived APO baseline appears to be more polluted than expected, and therefore the seasonal amplitudes may not be reliable. The seasonal amplitudes are higher than statistically-derived values and approach the value obtained at the Shetland islands (Wilson, 2013).

4.4 Atmospheric Events

I identified 11 positive APO excursions and five negative APO excursions of oceanic origin. Identification of events is limited by standard deviation; during periods of more variable data, events are less likely to be detected. For some events further analysis was not possible due to lack of data. The events analysed are presented in Table 4. Six productivity-related atmospheric events were identified within the time period of available satellite image data (March-October 2014). These events vary in duration and magnitude. The duration of events ranges from 2.5 hours to 15.6 hours and this is likely related both to the phytoplankton bloom and atmospheric transport. The magnitude of APO change during events ranges from 22.0 per meg to 57.3 per meg. The areas of influence for NPP events cover the whole baseline/ocean sector of the Mace Head air masses, showing that phytoplankton blooms are not limited to one area. However, with the small sample size available it is not possible to tell whether productivity events originate more frequently from a particular region.

Date	Duration (hours)	Δ APO (per meg)	Productivity (P)/ Ventilation (V)
04 March 2014	1.73	-15.47	V
05 April 2014	15.58	36.97	P
01 June 2014	5.90	44.51	P
02 July 2014	10.00	29.31	P
19 July 2014	2.50	35.69	P
19 August 2014	3.17	30.51	P
30 October 2014	2.17	21.98	P
02 November 2014	6.97	-26.82	V
12 January 2015	0.60	-36.61	V
14 January 2015	2.10	-29.95	V
04 February 2015	3.00	-32.95	V

Table 4: atmospheric events of oceanic origin including the duration of the event at Mace Head, the change in APO over that time and the ocean carbon cycle process that was determined to be the likely cause.

I identified five ventilation events within the dataset (Table 5). These events only occur between the months of November and March. The duration of the events ranges from 40 minutes to 7 hours. The magnitude of the APO change during the events ranges from -15 per meg to -37 per meg. The maximum magnitude of ventilation fluxes is smaller than the maximum magnitude of productivity-related fluxes. The areas of influence for the ventilation or upwelling events again cover a wide area of the ocean sector of Mace Head, however the small sample size limits the strength of conclusions.

There are also ten events not included in Table 5 that, based on the HYSPLIT air mass back trajectory, are of local origin but still show an APO excursion. The aim of my project is focussed on marine processes rather the terrestrial biosphere which will likely have a significant influence on these events, and therefore these events have not been analysed. This could potentially be a focus for future research. Studying these events could give insight into coastal ocean carbon cycle processes, although satellite data is often more difficult to obtain for coastal regions.

4.4.1 Seasonal distribution of atmospheric events

As mentioned above there is a seasonality in the distribution of events; ventilation events have been detected between November and March, and productivity events were detected between April and October. These conclusions are limited by gaps in the data and periods of high standard deviations, in addition and a lack of satellite data for NPP from November to February. Six positive APO excursions were detected between December 2014 and February 2015 which cannot be verified as productivity related due to the lack of satellite data. Therefore this distribution is not conclusive. However, ventilation is clearly seasonal and productivity events are concentrated in the spring and summer.

This seasonality is also evident in the magnitude of events. Figure 12 shows the mean Δ APO for the two types of events during each season. The seasonal distribution of events correlates well with the APO seasonal cycle, reflecting the dominant ocean carbon cycle process throughout the year. The largest productivity Δ APO occurs during spring. This is to be expected as the "spring bloom" of phytoplankton is a well documented phenomenon and increased temperatures and solar radiation lead to a rapid increase in productivity.

Photosynthesis is no longer limited by temperature or solar radiation and therefore the nutrients mixed into the surface waters during winter are utilised (Yamagishi et al., 2008). The summer months also have a high productivity related ΔAPO , which is likely due to the same phenomenon at more northerly latitudes; in sub-polar regions such as the Labrador Sea the "spring bloom" occurs during May and June (Körtzinger et al., 2008). This does not contest the seasonality observed in the ventilation events, as the Argo float data are available all year round.

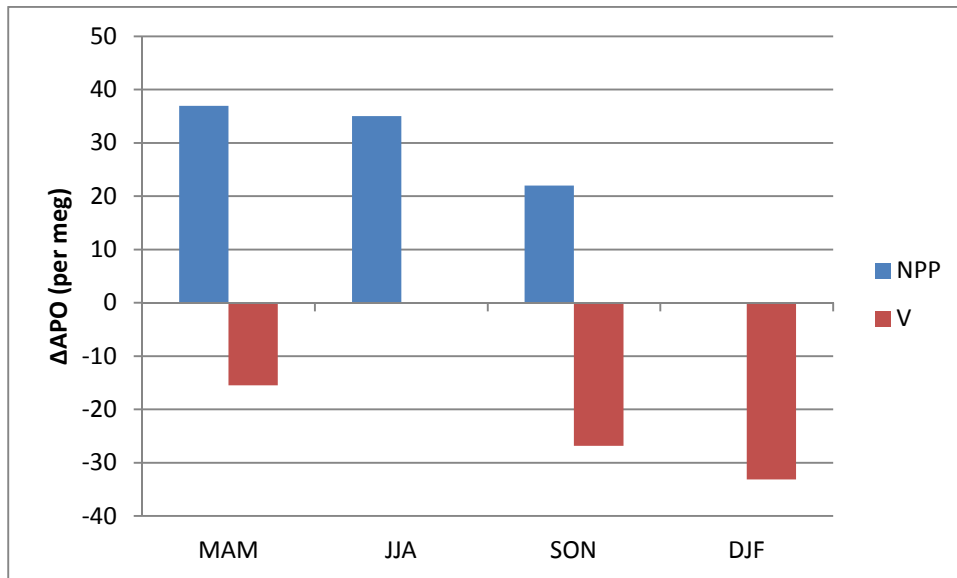


Figure 12: Mean change in APO (per meg) due to productivity (NPP, blue) and ventilation (V, red) events for each season.

The strongest ventilation events occur during the winter. High wind speeds and a deeper MLD lead to mixing of subsurface and surface waters. The subsurface waters are depleted in O_2 and rich in carbon and nutrients. This creates a drawdown of O_2 from the atmosphere to the ocean. Ventilation events also occur during the autumn and during the spring with a decreased magnitude. During the summer there are zero ventilation events. This is due to ocean stratification; a shallow MLD and relatively high SSTs prevent mixing and lead to surface waters with a low pCO_2 and supersaturated PO_2 (Patecki and Manning, 2007).

4.4.2 Oxidative ratios

Date	Oxidative ratio	R ²
Productivity		
05 April 2014	-3.34	0.74
01 June 2014	-14.01	0.45
02 July 2014	-0.47	0.02
09 July 2014	-3.74	0.51
19 August 2014	-2.33	0.47
30 October 2014	-1.37	0.87
Ventilation		
04 March 2014	1.98	0.02
02 November 2014	0.01	2×10^{-7}
12 January 2015	17.35	0.17
14 January 2015	-2.44	0.08
04 February 2015	-6.27	0.17

Table 5: Oxidative ratios (O₂:CO₂) and associated R² for all events

Table 5 shows that the oxidative ratios of both productivity and ventilation events have a wide range, and the strength of correlation varies greatly between events. In general, productivity events have higher R² values, indicating a stronger correlation between CO₂ and O₂ mole fractions than for ventilation events. The ratio values are quite similar, although three ventilation events are positive and all other ratios are negative. Thompson et al. (2007) suggest that positive oxidative ratios from ocean events are due to heat fluxes because this would have the same effect on both CO₂ and O₂ by changing the gas solubility of the sea water and therefore leading to outgassing or uptake of both gases, dependent on the direction of the change. Three of the ventilation events have positive oxidative ratios. The O₂ fluxes from the NEMO PlankTOM model (Blaine, 2005) were plotted, using the GoogleMapsPlot function within the R Openair package (Carslaw and Ropkins, 2012), for the dates of the back trajectories for the 04 March and 02 November events. NEMO PlankTOM data are not available for 2015, therefore this analysis cannot be used for the 12 January event. There is a relatively large heat flux within the region of the back trajectory for both events. For the 04 March event the heat flux does not account for the entire flux calculated from the observed APO change, therefore the change in dissolved oxygen concentration due to upwelling is still likely to have contributed. It is logical for the two effects to occur concurrently as the upwelled subsurface water as well as having a lower dissolved O₂ concentration, would also have a lower temperature. This could result in heat fluxes. The PFL data records a temperature of 3.87°C at the calculated MLD for the event (942 m) and a temperature of 5.19°C at 4 m depth. The 02 November event shows an equally large heat flux, however there is no correlation between O₂ and CO₂ (R² of 2.0×10^{-7}). This suggests that the other processes causing the observed APO excursion create a negative oxidation ratio which cancelled out the ratio due to the heat flux. As two further ventilation events have negative ratios, this seems plausible. In addition, ventilation events have a relatively low R² values, compared to productivity, which would occur if ventilation and heat fluxes are acting in opposition with regard to the oxidative ratio.

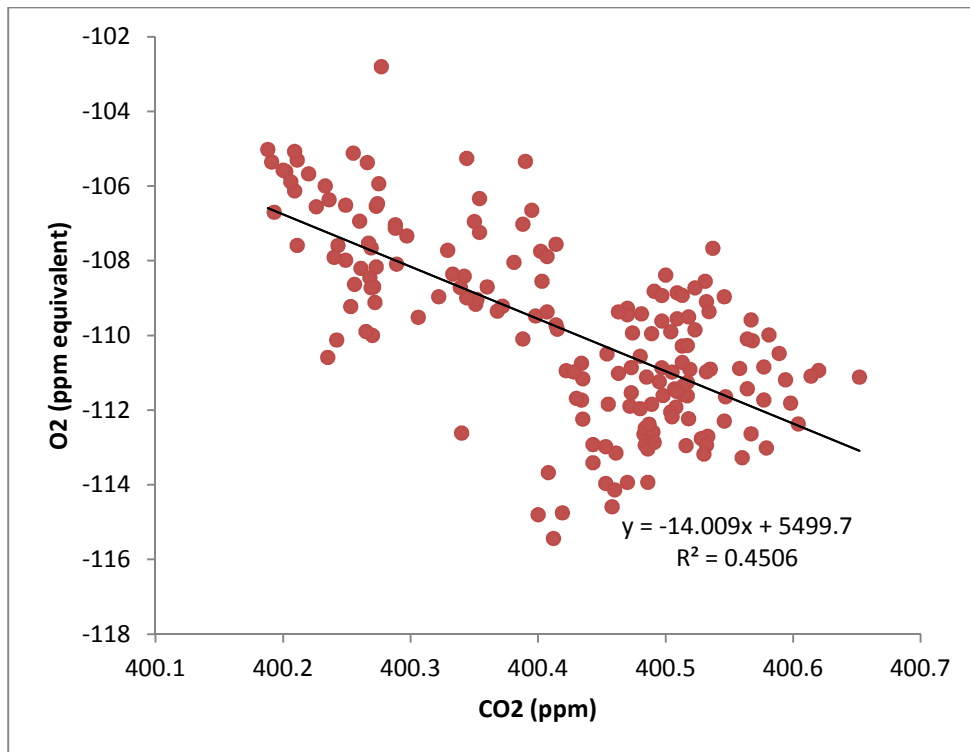


Figure 13: Oxidative ratio plot for the 01 June event. CO₂ is plotted against O₂ in ppm equivalent (ppmEq), which is calculated by dividing the O₂ value by 4.8. The least squares linear regression equation and associated R² are included.

All productivity events have negative ratios, which Thompson et al. (2007) also found. Photosynthesis causes O₂ outgassing and CO₂ uptake and therefore resulting in a negative O₂:CO₂ ratio. The observed APO change correlates strongly with the ratio; 01 June has the largest ratio (Figure 13) and the highest ΔAPO (-14 and 44 per meg respectively).

4.4.3 Productivity events

The fluxes resulting from the conceptual model and the Jacob (1999) puff equation (APO-derived) are presented in Table 6. There is a wide range in the accuracy in the output of the conceptual model. Some events, e.g. 01 June, have fluxes which match quite closely, however other events have a difference of an order of magnitude between the two fluxes. There is no correlation between the two flux estimates, or between the difference between the estimates and any particular parameter in the flux equation, however the events with the longest durations in general have the smallest discrepancies. These events are the 05 April event, which lasted 16 hours and 02 July event (10 hours duration). This is likely related to the use of 8 day average NPP images, as longer events will be more likely to significant within the 8 day average.

The events with the largest APO-derived fluxes are 09 July and 19 August. The APO-derived fluxes for these three events are an order of magnitude larger than all other NPP events. The events originate primarily from the west-south-west through to the north-north-west. This could suggest that strong blooms of phytoplankton occur in the northern Atlantic and southern Arctic oceans during this time period, although generally the height of marine productivity occurs earlier in the summer. Körtzinger et al. (2008) found a May/June spring bloom in the Labrador Sea, although more northerly latitudes could be slightly later. However, the satellite-derived fluxes are not of the same magnitude. The 19 August event

does have the second highest satellite derived flux, however this is still an order of magnitude smaller, and the 09 July event has a much smaller satellite derived flux. This suggests that either other processes are causing the observed flux, or that the flux equation causes a more severe over estimation of the flux in these particular cases. Local coastal carbon cycle processes, which are poorly resolved by satellite imagery, may also be contributing to the observed APO excursions. Alternatively the conceptual model may be underestimating the flux in these cases. The area of the ocean over which the phytoplankton bloom or other productivity event is occurring has not been taken into account in my calculations, however it would logically impact the observed APO change at Mace Head. Using the maximum NPP value within the back trajectory may balance this out slightly, however this could account for the larger magnitude of the sea-air flux using the APO values. Visual analysis suggests this may be the case for the 09 July and 19 August events, however a more precise method should be developed in future research.

Date	Modelled flux (mg C m ⁻² day ⁻¹)	Observed APO derived flux (mg C m ⁻² day ⁻¹)	Difference (modelled flux - APO-derived flux) (mg C m ⁻² day ⁻¹)
05 April 2014	2085	1143	942
01 June 2014	3886	2354	1532
02 July 2014	5113	5038	75
09 July 2014	2674	39,197	-36,523
19 August 2014	7826	60,133	-52,307
30 October 2014	8669	4749	4120

Table 6: Productivity events and the O₂ air-sea flux calculated from the conceptual model and from the observed ΔAPO at Mace Head, and the difference between these two fluxes.

NEMO-PlankTOM heat fluxes were added to the conceptual model in order to investigate whether they may have contributed to the observed ΔAPO (Table 6). Overall heat fluxes do not appear to have contributed to these events, which agrees with the oxidative ratios discussed above. Instead heat fluxes appear to be contributing to O₂ outgassing, alongside photosynthesis, therefore increasing the discrepancy between modelled and APO-derived fluxes. The two exceptions are 09 July and 19 August, which have the two largest APO-derived fluxes. For these two events, including the heat fluxes does reduce the difference between the two fluxes, however the model still does not explain the full magnitude of the event.

For three productivity events I was able to use NAME air mass footprints in addition to HYSPLIT back trajectories. NAME is a much more complex atmospheric transport model and should therefore improve the accuracy of the conceptual model. All NAME outputs are different from the respective HYSPLIT outputs, although the different areas of influence only appear to have a significant impact on the modelled results of one event. The NAME footprint for the 05 April event is the most similar to the HYSPLIT trajectory; the wind direction is 10-20° different, however it is still focussed over a relatively small area. The NAME footprint for 06 April looks more similar to the HYSPLIT back trajectory for 05 April. This could be due to the difference in temporal resolution or other parameters of the meteorological data used between NAME and HYSPLIT. The 01 June outputs follow a

similar pattern; the back trajectory and footprint are both focussed over a small area, however the actual area of influence and path of approach are some degrees apart. The NAME footprint for 02 July is however much more dispersed than the HYSPLIT trajectory for the same event. The fetch is therefore longer, however this has a negligible influence on flux calculations. Nevertheless the two areas of influence do intersect. These comparisons illustrate two differences in the modelling and data used. The first two events show a difference in wind direction causing a different area of influence to be modelled and the latter event suggests changes in wind speed in addition to wind direction and perhaps turbulence in the NAME model.

In terms of effects on the modelled mass flux, the 02 July event is most effected as the NAME footprint covers a wider area and within that area of influence is a higher maximum modelled flux of approximately $10,000 \text{ mg C m}^{-2} \text{ day}^{-1}$. This is almost $4000 \text{ mg C m}^{-2} \text{ day}^{-1}$ higher than that calculated from the HYSPLIT trajectory. Although the fetch is longer, this has only a small effect on the flux equation. The average wind speed is almost unchanged. Therefore the difference between the APO-derived flux and the modelled flux is approximately $4000 \text{ mg C m}^{-2} \text{ day}^{-1}$ larger. In contrast, the NAME footprint for the 01 June event produces a lower modelled maximum flux of $3062 \text{ mg C m}^{-2} \text{ day}^{-1}$ (compared to $4796 \text{ mg C m}^{-2} \text{ day}^{-1}$ for the HYSPLIT trajectory). The average wind speed over the NAME footprint is 2 m s^{-1} lower which when rounded appropriately produces the same APO-derived NPP as the HYSPLIT back trajectory. The 05 April event again produces a lower modelled flux as the angle of approach, which means that the area of highest productivity is not within the area of influence. Therefore there is less discrepancy between the modelled and APO-derived flux values. These results do show how a more complex atmospheric transport model can have an effect on the flux output. However, given the discrepancies between the modelled and APO-derived fluxes it is difficult to make clear conclusions. It is suggested that future work should involve NAME or similar atmospheric transport models.

NAME outputs have an advantage in that they are continuous fields whereas HYSPLIT back trajectories, are point type files, rather than vector lines. Therefore when calculating statistics from intersected fields, the values may not be a true representation, depending on the resolution of the data. For Argo floats data where the resolution is very coarse this will have little effect, however data such as the NOAA sea winds and the NPP have much higher resolution and so pixels may be missed in calculating statistics.

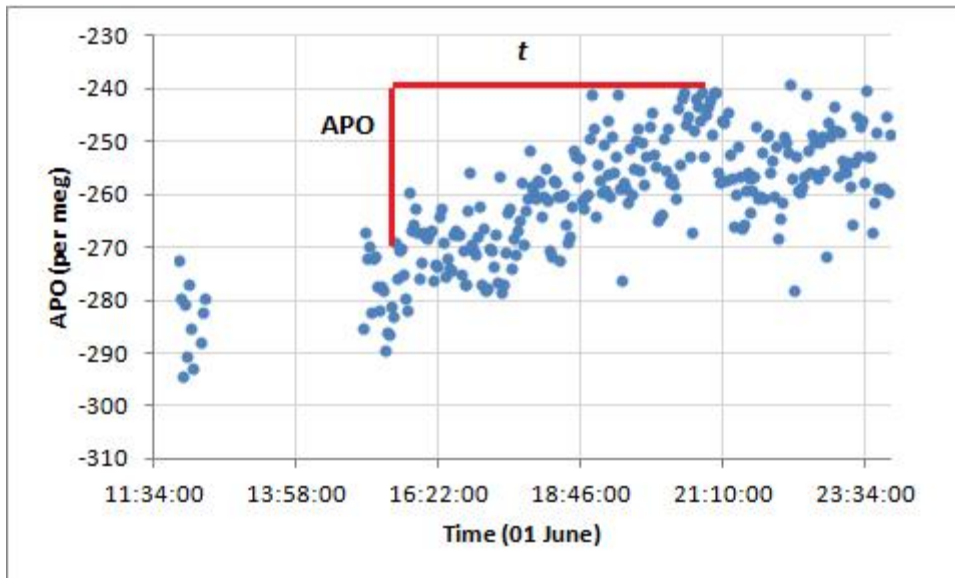


Figure 14: Plot of 2 minute averaged APO data during 01 June, showing the duration and magnitude of the event.

I use the example of the 01 June event to work through the full analysis undertaken for every event. When the event has been identified visually, the exact duration and Δ APO are calculated from the two minute data (Figure 14). The event is defined as from 15:06 until 21:00, a duration of 5.9 hours, with a Δ APO of 44.51 per meg. The event is characterised by a continuous increase of O_2 mole fraction and a CO_2 mole fraction that increases slightly and then decreases. HYSPLIT is then run to produce an air mass back trajectory to confirm an ocean origin of the air masses. Initially a 96 hour trajectory is run. This trajectory is imported into the SeaDAS software and overlaid onto the appropriate eight day average NPP image (Figure 15). Figure 15 shows a large area of high NPP in the ocean surrounding Mace Head, and the back trajectory intersects with this. I used SeaDAS to calculate the mean and maximum NPP that the back trajectory intersects with. I followed a version of the Yamagishi et al. (2008) method of estimating the NPP from the satellite image. Yamagishi et al. (2008) took the difference between the bloom NPP and the surrounding NPP i.e. the change in NPP, to be comparable to the change in observed APO at the station. This is difficult to keep consistent and also not possible to calculate for a wider area in SeaDAS. As an approximation of this method I take the difference between the maximum NPP and the mean NPP within the back trajectory area. For 01 June this gives an NPP value $4796 - 910 = 3886 \text{ mg C m}^{-2} \text{ day}^{-1}$.

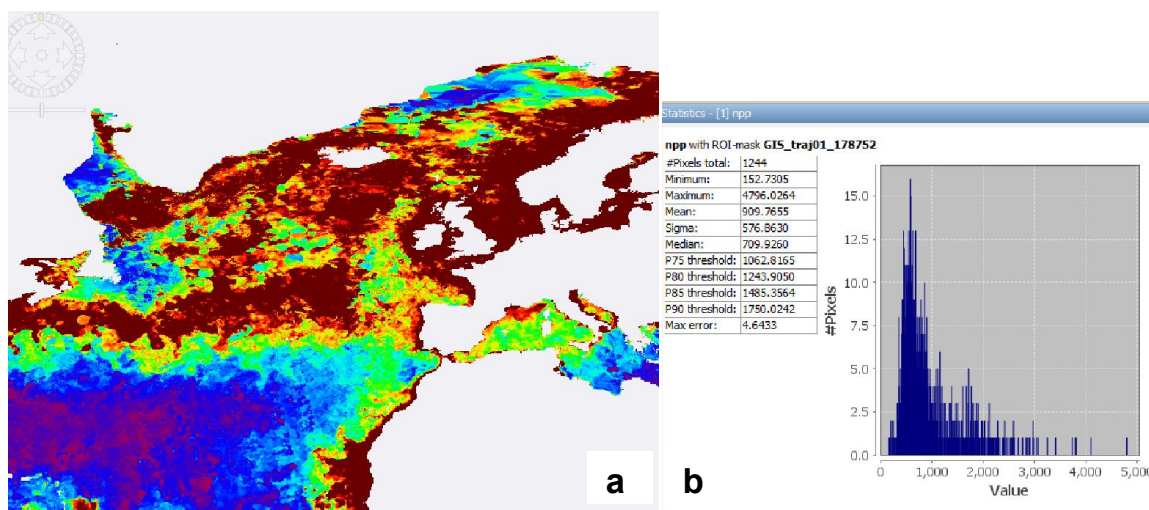


Figure 15: a) NPP derived from ocean colour satellite data modelled with the VGPM for 25/05/2014 to 01/06/2014. b) screen capture from SeaDAS software showing the statistics calculated for the pixels in the NPP image which intersected by the 01 June back trajectory.

The APO-derived flux is then calculated using Equation 3. This assumes that the change in APO is entirely due to productivity-related ocean processes, a reasonable assumption on short timescales (unless it is due to another ocean process). This involves calculating the mean wind speed within the back trajectory from the NOAA sea winds dataset (11.9 m s^{-1}), the PBL from HYSPLIT (60 m) and the wind fetch from the back trajectory in Google Earth (2800 km). The resulting value has to be converted into a value comparable to the NPP, from $\text{mol m}^{-2} \text{ yr}^{-2}$ to a mass flux in units of $\text{mg C m}^{-2} \text{ day}^{-1}$. The resulting flux is $2354 \text{ mg C m}^{-2} \text{ day}^{-1}$. This flux is $1531 \text{ mg C m}^{-2} \text{ day}^{-1}$ smaller than the flux produced by the satellite data. Yamagishi et al. (2008) found that their APO-derived flux estimates came within an order of magnitude of the satellite image derived fluxes, so this discrepancy is not uncommon, however other processes could also be affecting the ocean carbon cycle. Changes in temperature causes the solubility of gases in water to alter, which can lead to gas fluxes. The O_2 fluxes produced from the NEMO PlankTOM model can be used to further refine the modelled flux. A maximum value of $-0.1 \text{ mol m}^{-2} \text{ day}^{-1}$ occurs during the back trajectory. The negative flux denotes an air-to-sea flux, i.e. uptake of O_2 from the atmosphere. This flux is in the opposite direction to the flux due to productivity and therefore may partly cancel out the increase in atmospheric O_2 (and therefore APO). Once all fluxes are converted into comparable units, this gives a flux of $0.35 \text{ mol m}^{-2} \text{ day}^{-1}$ from the combination of ocean colour and NEMO PlankTOM data, compared to a flux of $0.27 \text{ mol m}^{-2} \text{ day}^{-1}$ calculated from the observed APO. This results in a much smaller difference in magnitude of the flux.

4.4.4 Ventilation events

The fluxes resulting from the ventilation conceptual model and the fluxes derived from ΔAPO and the Jacob (1999) puff equation are presented in Table 7. The modelled flux in Table 7 is calculated using the mean ΔpO_2 calculated from the two methods (typical monthly dissolved O_2 concentration and real time float data). The two different methods of calculating ΔpO_2 produce very similar results with differences of less than 1 mL L^{-1} . In all but one case (02 November) the ΔpO_2 calculated using typical monthly dissolved O_2 concentrations is less than those calculated using the real time data. The differences in the calculated fluxes are small, therefore suggesting that typical monthly concentrations can be used without any significant loss of accuracy in the model. The modelled flux is, except for one outlier, always greater than the APO-derived flux. There is no correlation between the two fluxes.

Date	APO-derived flux (mol m ⁻² day ⁻¹)	Conceptual model flux (mol m ⁻² day ⁻¹)	Difference (mol m ⁻² day ⁻¹)
04 March 2014	-3.81	-11.10	14.92
02 November 2014	-1.38	-6.36	7.73
12 January 2015	-40.72	-5.06	45.78
14 January 2015	-2.78	-5.09	7.87
04 February 2015	-2.13	-8.03	10.17

Table 7: Ventilation events and the O₂ air-sea flux calculated from the conceptual model and from the observed ΔAPO at Mace Head, and the difference between these two fluxes.

As discussed above, ventilation events are highly seasonal as they are driven by high wind speeds and a deep mixed layer which brings O₂-depleted waters to the surface. Based on this understanding of ventilation events, we might expect the magnitude of the flux to be correlated with wind parameters. There is no correlation between APO-derived flux and wind speed, or fetch. There is some correlation between modelled flux and wind speed, with a greater flux occurring at higher wind speeds. The exception to this pattern is the 14 January event which has a flux approximately equal to 12 January despite an average wind speed of 6 m s⁻¹ higher. There is no correlation between modelled flux and fetch. The conceptual model fluxes do correlate with MLD, with the exception of 02 November 2014, however the APO-derived fluxes do not. This suggests that there is a complexity in the system which drives the ΔAPO observed at Mace Head which is not captured in the model. This could be related to the atmospheric transport, or the simplistic way of viewing the pO₂ changes caused by upwelling. As with the productivity events, the area of deep MLD could be related.

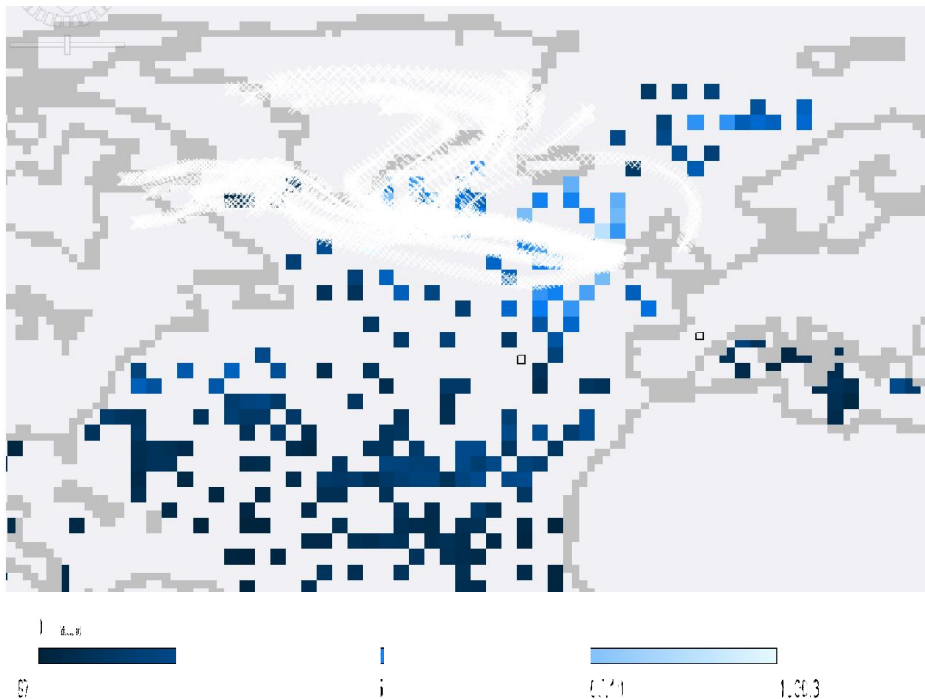


Figure 16: MLD dataset for 04 March 2014, with the back trajectory overlaid, produced in SeaDAS.

The ventilation event on 04 March 2014 will be used as an example of the full event analysis undertaken. I visually identify the event and calculate the duration and change in APO as described above for productivity events. Similarly HYSPLIT is run to produce an air mass back trajectory to confirm an ocean origin of the air masses. This is overlaid with the Hosada et al. (2010) MLD estimates, using the SeaDAS software (Figure 16). I take the mean of the

two MLD estimates; 716 m and 1169 m, giving a mean of 942.5 m. Using the World Ocean Atlas climatology I calculate the change in dissolved O₂ between a MLD of 942.5 m and the surface during a typical March within the back trajectory. The climatology is averaged to standard depth levels and so the depth is slightly approximated; 950 m is used. The resulting change is -0.673 mL L⁻¹. I use the ODV software to select profiling floats within the dates of the back trajectory. In this case there is only one float within the back trajectory area, on 01 March. I calculate the change in dissolved O₂ between a depth of 942.5 m and the surface (4 m for this float), which is -0.84 mL L⁻¹. I use the Garcia and Keeling (2001) and Wanninkopf (1992) equation (Equation 5) to calculate the air-sea flux that would result from these changes in dissolved O₂. This involves calculating the mean SST and salinity within the back trajectory area from the Hosada et al. (2010) dataset. The resulting flux is -11.1 mol m⁻² day⁻¹. I calculate the APO derived flux as described for productivity events: -3.81 mol m⁻² day⁻¹. The discrepancy between the two fluxes is 7.29 mol m⁻² day⁻¹. Including the heat flux increases the discrepancy by 1 mol m⁻² day⁻¹ because the upwelling of cold water increases the gas solubility and therefore the uptake of O₂, in addition to the effect of the change in dissolved O₂ concentration.

5. Conclusions

The aim of this project was to use continuous atmospheric measurements of CO₂ and O₂ collected at Mace Head to investigate the seasonal cycles and short term ocean carbon cycle events. This was achieved using curve fitting programs to determine the detrended seasonal cycle and calculate the seasonal cycle amplitudes. I detected atmospheric events using the observed APO, air mass back trajectories and satellite image derived estimates of NPP and Argo float estimates of the MLD. I created conceptual models of productivity events and ventilation events and tested these against the observed events at Mace Head.

5.1 Summary of key findings

1. The season cycle amplitudes of the CO₂, O₂ and APO data are 17.78 ppm, 149 per meg and 76.57 per meg respectively. The APO seasonal cycle amplitude is slightly larger than half of the amplitude of the O₂ seasonal cycle. The CO₂ minimum occurs in August and the maximum in April. The O₂ seasonal cycle is almost exactly the inverse: the maximum occurs in August however the minimum is in March. The APO seasonal cycle peaks in July and the minimum is in February. The timings of the seasonal cycles agree with previous Mace Head data (Sirignano et al., 2010). The CO₂ amplitude is larger than any recent data from European stations. The O₂ seasonal amplitude is similar to the previous Mace Head value (142 ±6 per meg) and the F3 Oil Platform (144 ±2). The APO seasonal amplitude is similar to the previous Mace Head value, based on flask measurements, although slightly lower perhaps suggesting that there is less ocean variability in this particular year than the average year.
2. Six productivity related atmospheric events and five ventilation related events were identified within the dataset. There is seasonality in the magnitude of the two types of events. This correlates well with the APO seasonal cycle; high productivity during spring and summer and strong ventilation/upwelling events during winter. (Note that the lack of satellite ocean colour data for the northern Atlantic means that no productivity events could be detected during winter).
3. The oxidative ratios for atmospheric events are mostly negative because the carbon cycle processes involved in upwelling and productivity produce fluxes of O₂ and CO₂ that move in opposite directions. There are two events with positive oxidative ratios which may be due to heat fluxes; changes in the solubility act on CO₂ and O₂ to produce fluxes in the same direction. I used NEMO PlankTOM modelled O₂ fluxes to investigate this for the 04 March event. There is a relatively high flux compared to the surrounding area during this event of 1 mol m⁻² day⁻¹. Both events with a positive oxidative ratio are ventilation events, which are associated with a change in temperature alongside the change in dissolved O₂ concentration and therefore it is likely that this sometimes results in heat fluxes. No defining characteristics of the events when this occurs can be determined based on the small sample size of two.
4. The air-sea fluxes required to generate the observed APO excursions at Mace Head were calculated. Overall productivity related events have a higher observed change in APO and the magnitude of the required flux is also therefore larger.

5. I have used a conceptual model to investigate productivity-related events using HYSPLIT and NAME air mass back trajectories and satellite ocean colour data. In four out of the six events the conceptual model fits the observed APO change well, producing a flux within the same order of magnitude as the APO-derived flux. The other two events (09 July and 19 August) have modelled fluxes that are an order of magnitude larger than the APO-derived fluxes. This is similar to previous studies which used similar methodologies. I used the NEMO PlankTOM modelled heat flux data to investigate whether adding O₂ fluxes due to heat fluxes improved the conceptual model. For the two events with the largest discrepancy between fluxes (09 July and 19 August), including the heat fluxes does improve the model, however there is still a larger discrepancy than for any other events. In the majority of cases, including the heat fluxes within the model increases the difference between APO-derived and modelled fluxes, as they drive sea to air fluxes of O₂.
6. I used a conceptual model to investigate ventilation-related atmospheric events, consisting of the HYSPLIT back trajectories, Argo MLD and dissolved O₂ concentrations from Argo data. The modelled flux is, except for one outlier, always greater than the APO-derived flux. Heat flux data is only available for 2014, therefore this could not be analysed for the majority of the ventilation events. For 04 March and 02 November the heat fluxes reinforce the direction of the conceptual model flux and therefore increase the difference between the conceptual model flux and the APO-derived flux. The model corresponds relatively well to the observed APO fluxes for all but one event.

5.2 Limitations of the research

The conclusions of this project are limited by the short term dataset which restricts the number of events available for analysis. All conclusions are based on a small sample size. I have considered several refinements to the methods used here which were not able to be implemented, and these may have increased the precision of flux calculations.

5.3 Suggestions for further research

I would suggest continuing this analysis on longer datasets and improving the methods of calculating both the APO-derived flux and the modelled flux by using NAME air mass back trajectories and investigating the effect of the area of productivity or MLD change in the ocean. N₂O fluxes have been used by Nevison et al. (2012) to model the contribution of ventilation to events. This allows calculation of the productivity signal as a residual independent of the satellite ocean colour data. I suggest that this method is used in future research. My project has focussed solely on ocean carbon cycle processes however there is the opportunity for future research into coastal processes and the European fossil fuel signal.

Reference List

- Argo Science Team, 2001. Argo: The global array of profiling floats. p. 248–258. In: Observing the Oceans in the 21st Century, ed. by C. J. Koblinsky and N. R. Smith, GODAE Project Office, Bureau of Meteorology, Melbourne.
- Barningham, T., 2013, Detection and attribution of carbon cycle processes from atmospheric O₂ and CO₂ observations at Baring Head, New Zealand. MSc thesis, University of East Anglia.
- Behrenfeld, M.J. and Falkowski, P.G., 1997. Photosynthetic rates derived from satellite-based chlorophyll concentrations. *Limnology and Oceanography*, 42(1), pp.1-20.
- Blaine, T.W., 2005, Continuous measurements of atmospheric Ar/N₂ as a tracer of air-sea heat flux: models, methods and data, PhD thesis, University of California.
- Bousquet, P., Gaudry, A., Ciais, P., Kazan, V., Monfray, P., Simmonds, P. G., Jennings, S. G., and O'Connor, T. C., 1996. Atmospheric CO₂ concentration variations recorded at Mace Head, Ireland, from 1992 to 1994, *Physics and Chemistry of the Earth*, 21, pp.477–481.
- Broecker, W. S. and Peng, T.-H., 1982. *Tracers in the Sea*. New York: Eldigio Press.
- Carlaw, D.C. and Ropkins, K., 2012. openair — an R package for air quality data analysis. *Environmental Modelling & Software*, 27-28, pp. 52-61.
- Cleveland, R.B., Cleveland, W.S., McRae, J.E., and Terpenning, I., 1990. STL: A seasonal trend decomposition procedure based on loess. *Journal of Official Statistics*, 6(1), 3-73.
- Derwent, R.G., Ryall, D.B., Manning, A.J., Simmonds, P.G., O'Doherty, S., Biraud, S., Ciais, P., Ramonet, M. and Jennings, S.G., 2002. Continuous observations of carbon dioxide at Mace Head, Ireland from 1995 to 1999 and its net European ecosystem exchange. *Atmospheric Environment*, 36, pp.2799-2807.
- Doney, S.C., Fabry, V.J., Feely, R.A. and Kleypas, J.A., 2008. Ocean Acidification: The Other CO₂ Problem. *Annual Review of Marine Science*, 1, pp.169-192.
- Dong, S., Sprintall, J., Gille, S.T. and Talley, L., 2008. Southern Ocean mixed-layer depth from Argo float profiles. *Journal of Geophysical Research*, 11, C06013.
- Draxler, R.R. and Hess, G.D., 1998. An overview of the HYSPLIT_4 modelling system for trajectories, dispersion and deposition. *Australian Meteorological Magazine*, 47, pp.295-308. Available at: http://ready.arl.noaa.gov/HYSPLIT_traj.php
- Fang, S.X., Tans, P.P., Steinbacher, M., Zhou, L.X. and Luan, T., 2015, Study of the regional CO₂ mole fractions filtering approach at a WMO/GAW regional station in China. *Atmospheric Measurement Techniques: Discussions*, 8, pp.7057-7091.
- Fleming, Z.L., Monks, P.S. and Manning, A.J., 2012. Review: untangling the influence of air-mass history in interpreting observed atmospheric composition. *Atmospheric Research*, 104-105, pp.1-39.
- Garcia, H.E. and Gordon, L.I., 1992. Oxygen solubility in seawater: better fitting equations, *Limnology and Oceanography*, 37, pp.1307-1312.
- Garcia, H.E., and Keeling, R.F., 2001. On the global oxygen anomaly and air-sea flux, *Journal of Geophysical Research-Oceans*, 106, pp.31155-31166.
- GeoBasis-DE/BKG, 2015. Google maps imagery.

- Google, 2009. Google maps imagery.
- Google Earth, 2015. Available at: <http://www.google.com/earth/index.html>
- Hosada, S., Ohira, T., Sato, K. and Suga, T., 2010. Improved description of global mixed-layer depth using Argo profiling floats. *Journal of Oceanography*, 66, pp.773-787.
- IPCC, 2007. *Climate Change 2007: The Physical Science Bases. Contribution of Working Group I to the Fourth Assessment Report of the Intergovernmental Panel on Climate Change, 2007*, Solomon, S., D. Qin, M. Manning, Z. Chen, M. Marquis, K.B. Averyt, M. Tignor and H.L. Miller (eds.). Cambridge: Cambridge University Press.
- IPCC, 2013. *Climate Change 2013: The Physical Science Basis. Contribution of Working Group I to the Fifth Assessment Report of the Intergovernmental Panel on Climate Change*, Stocker, T.F., Qin, D., Plattner, G.-K., Tignor, M., Allen, S.K., Boschung, J., Nauels, A., Xia, Y., Bex, V. and Midgley, P.M. (eds.). Cambridge: Cambridge University Press.
- International Argo Program, 2015 [online] *Argo: part of the integrated global observation strategy* Available at: <http://www.Argo.ucsd.edu/index.html> [Accessed 25/02/2015].
- Jacob, D. 1999. *An Introduction to Atmospheric Chemistry*. Princeton : Princeton University Press.
- Jones A., Thomson, D., Hort, M. and Devenish, B., 2007, The U.K. Met Office's next-generation atmospheric dispersion model, NAME III, in Borrego, C. and Norman, A.-L. (Eds). *Air Pollution Modeling and its Application XVII (Proceedings of the 27th NATO/CCMS International Technical Meeting on Air Pollution Modelling and its Application)*, Springer, pp. 580-589.
- Keeling, C.D., 1960. The Concentration and Isotopic Abundances of Carbon Dioxide in the Atmosphere. *Tellus*, 12(2), pp. 200-203.
- Keeling, C.D., Bacastow, R.B., Carter, A.F., Piper, S.C., Whorf, T.P., Heimann, M., Mook, W.G. and Roeloffzen, H., 1989. A three-dimensional model of atmospheric CO₂ transport based on observed winds: 1. Analysis of observational data. *Geophysical Monograph*, 55.
- Keeling, R.F. and Manning, A.C., 2014. Studies of Recent Changes in Atmospheric O₂ Content. In: *Treatise on Geochemistry 2nd Edition*. Turekian, K.K., Keeling, R.F. and Russell, L.M., Elsevier Limited, Oxford.
- Keeling, R.F. and Schertz, S.R., 1992. Seasonal and interannual variations in atmospheric oxygen and implications for the global carbon cycle. *Nature*, 358, pp.723-727.
- Karleskind, P., Lévy, M. and Memery, L., 2011. Subduction of carbon, nitrogen, and oxygen in the northeast Atlantic. *Journal of Geophysical Research*. 116, C02025.
- Körtzinger, A., Send, U., Wallace, D.W.R., Karstensen, J. and DeGrandpre, M., 2008. Seasonal cycle of O₂ and pO₂ in the central Labrador Sea: Atmospheric, biological, and physical implications. *Global Biogeochemical Cycles*, 22, GB1014.
- Kozlova, E.A., Manning, A.C., Kisilyakhov, Y., Siebert, T. and Heimann, M., 2008, Seasonal, synoptic, and diurnal-scale variability of biogeochemical trace gases and O₂ from a 300-m tall tower in central Siberia. *Global Biogeochemical Cycles*, 22, GB4020.
- Laws, E. A.: Photosynthetic Quotients, New Production and Net Community Production in the Open Ocean, *Deep-Sea Res.*, 38(1), 143–167, 1991.

- Locher, R. and Ruckstuhl, A. et al., 2012. IDPmisc: Utilities of Institute of Data Analyses and Process Design (www.idp.zhaw.ch). R package version 1.1.17. <http://CRAN.R-project.org/package=IDPmisc>
- Lueker, T. J., 2004. Coastal upwelling fluxes of O₂, N₂O, and CO₂ assessed from continuous atmospheric observations at Trinidad, California, *Biogeosciences*, 1, pp.101-111.
- Manning, A.J., O'Doherty, S., Jones, A.R., Simmonds, P.G. and Derwent, R.G., 2011. Estimating UK methane and nitrous oxide emissions from 1990 to 2007 using an inversion modeling approach. *Journal of Geophysical Research*, 116(D02305), pp.1-19.
- Nevison, C.D., Keeling, R.F., Kahru, M., Manizza, M., Mitchell, B.G. and Cassar, N., 2012. Estimating net community productivity production in the Southern Ocean based on atmospheric potential oxygen and satellite ocean colour data. *Global Biogeochemical Cycles*, 26, GB1020.
- NOAA, 2015. Blended Sea Wind Dataset. Available at: <https://www.ncdc.noaa.gov/data-access/marineocean-data/blended-global/blended-sea-winds>
- Ocean Data View v.4.7.3, 2015. Available at: <http://odv.awi.de>
- Oregon State University, 2014. *Ocean Productivity* [online] Available at: <http://www.science.oregonstate.edu/ocean.productivity/index.php> [Accessed 28/10/14].
- Patecki, M. and Manning, A.C., 2007. First results from shipboard atmospheric O₂ and CO₂ measurements over the North Atlantic Ocean. *Oceans 2007- Europe*. 061215-111.
- Pickers, P.A. and Manning, A.C., 2015. Investigating bias in the application of curve fitting programs to atmospheric time series. *Atmospheric Measurement Techniques*, 8, pp.1469-1489.
- Press, W.H., Teukolsky, S.A., Vetterling, W.T. and Flannery, B.P., 1986. Numerical Recipes in Fortran 90. The Art of Parallel Scientific Computing, 2nd Edition, Cambridge University Press.
- R Development Core Team (2008). R: A language and environment for statistical computing. R Foundation for Statistical Computing, Vienna, Austria. ISBN 3-900051-07-0, Available at: <http://www.R-project.org>.
- Reinsch, C.H., 1967. Smoothing by spline functions, *Numerische Mathematik*, 10, pp.177-183.
- Ruckstuhl, A.F., Jacobsen, M.P., Field, R.W. and Dodd, J.A., 2001, Baseline subtraction using local regression estimation. *Journal of Quantitative Spectroscopy & Radiative Transfer*, 68, pp.179-193.
- Ruckstuhl, A.F., Henne, S., Reimann, S., Steinbacher, M., Vollmer, M.K., O'Doherty, S., Buchmann, B. and Hueglin, C., 2012. Robust extraction of baseline signal of atmospheric trace species using local regression. *Atmospheric Measurement Techniques*, 5, pp.2613-2624.
- Ryall, D.B. and Maryon, R.H., 1998. Validation of the UK Met. Office's name model against the ETEX dataset. *Atmospheric Environment*, 32, 4265-4276.
- Sabine, C.L., Feely, R.A., Key, R.M., Lee, K., Bullister, J.L., Wanninkhof, R., Wong, C.S., Wallace, D.W.R., Tilbrook, B., Millero, F.J., Peng, T-H., Kozyr, Ono, T. and Rois, A.F., 2004. The oceanic sink for anthropogenic CO₂. *Science*, 305(5682), pp.367-371.
- SeaDAS 7.2, 2015. Available at: <http://seadas.gsfc.nasa.gov/installers/>

- Sirignano, C., Neubert, R.E.M., Rödenbeck, C. and Meijer, H.A.J., 2010. Atmospheric oxygen and carbon dioxide observations from two European coastal stations 2000–2005: continental influence, trend changes and APO climatology. *Atmospheric Chemistry and Physics*, 10, pp.1599-1615.
- Stephens, B.B., Keeling, R.F., Heimann, M., Six, K.D., Murnane, R. and Caldeira, K., 1998. Testing global ocean carbon cycle models using measurements of atmospheric O₂ and CO₂ concentration. *Global Biogeochemical Cycles*, 12, pp.213–230.
- Thompson, R.L., Manning, A.C., Gloor, E., Schultz, U., Seifert, T., Hänsel, F., Jordan, A. and Heimann, M., 2009. In-situ measurements of oxygen, carbon monoxide and greenhouse gases from Ochsenskopf tall tower in Germany. *Atmospheric Measurement Techniques*, 2, pp.573-591.
- Thompson, R.L., Manning, A.C., Lowe, D.C. and Weatherburn, D.C., 2007. A ship-based methodology for high precision atmospheric oxygen measurements and its application in the Southern Ocean region, *Tellus*, pp.1-11.
- Thoning, K.W., Tans, P.P. and Komhyr, W.D., 1989. Atmospheric carbon dioxide at Mauna Loa Observatory 2. Analysis of the NOAA GMCC data, 1974–1985. *Journal of Geophysical Research.- Atmospheres*, 94, pp.8549–8565.
- van der Laan, S., van der Lann-Luijkx, I.T., Rödenbeck, C., Varlagin, A., Shironya, I., Neubert, R.E.M., Ramonet, M. and Meijer, H.A.J., 2014. Atmospheric CO₂, δ(O₂/N₂), APO and oxidative ratios from aircraft flask samples over Fyodorovskoye, Western Russia. *Atmospheric Environment*, 97, pp.174-181.
- van der Laan-Luijkx, I.T., Neubert, R.E.M., van der Lann, S. and Meijer, H.A.J., 2010. Continuous measurements of atmospheric oxygen and carbon dioxide on a North Sea gas platform. *Atmospheric Measurement Techniques*, 3, pp.113-125.
- Wanninkhof, R., 1992. Relationship between wind-speed and gas-exchange over the ocean, *Journal of Geophysical Research-Oceans*, 97, pp.7373-7382.
- Wilson, P., 2013. Insight into the carbon cycle from continuous measurements of oxygen and carbon dioxide at Weybourne Atmospheric Observatory, UK. PhD thesis, University of East Anglia.
- World Ocean Atlas, 2013, Dissolved O₂ Dataset. Available at: <https://www.nodc.noaa.gov/OC5/woa13/woa13data.html>
- World Ocean Database, 2015, Argo data, Available at: <https://www.nodc.noaa.gov/OC5/WOD13>
- Yamagishi, H., Tohjima, Y., Mukai, H. and Sasaoka, K., 2008. Detection of regional scale sea-to-air oxygen emission related to spring bloom near Japan by using in-situ measurements of the atmospheric oxygen/nitrogen ratio. *Atmospheric Chemistry and Physics*, 8, pp.3325-3335.
- Zhang, H.-M., Bates, J.J. and Reynolds, R.W., 2006a. Assessment of composite global sampling: Sea surface wind speed, *Geophysical Research Letters*, 33, L17714.
- Zhang, H.-M., Reynolds, R.W. and Bates, J.G., 2006b. Blended and gridded high resolution global sea surface wind speed and climatology from multiple satellites: 1987–present. 14th Conference on Satellite Meteorology and Oceanography, Atlanta, GA, *American Meteorological Society*, Paper 100004.